Towards Coherent Control of a Single Cs Atom in an Ultracold Rb Cloud

von
Farina Kindermann

Masterarbeit in Physik

angefertigt am
Institut für Angewandte Physik

vorgelegt der
Mathematisch-Naturwissenschaftlichen Fakultät
der Rheinischen Friedrich-Wilhelms-Universität Bonn

September 2011

1. Gutachter: Prof. Dr. Dieter Meschede
2. Gutachter: Prof. Dr. Artur Widera

Contents

1 Introduction

The development of the laser cooling technique [1] as well as the method of evaporative cooling [2] allows to investigate temperature regions where quantum mechanical effects are dominant. Since then, preparation, manipulation and detection of a well defined quantum state have become easy to implement. In 1995 the groups of W. Ketterle, E.A. Cornell and C.E. Wieman realised the first experimental Bose-Einstein Condensates using alkali metal atoms [3, 4]. This breakthrough motivated a tremendous increase of experiments in this field.

The experiments evolved from the interference of coherent matter waves [5] and the atom laser [6] over observation of quantised vortices [7] as proof for the BECs superfluidity to the point when condensates consisting of magnons[8] or photons[9] were realised. Furthermore, many phenomena in nature such as superfluidity [10] or formation of dimers [11] and trimers [12] rely on the interaction between particles. This is also the case for Feshbach resonances [13, 14], which allow to manipulate the interaction strength in a controlled way. In the beginning the interest was mainly focussed on interactions between atoms of the same element, but nowadays more experiments investigate mixtures of different atom species, so called heteronuclear mixtures. In 2002 a double condensate of ^{39}K atoms and ^{87}Rb atoms was realised in a magnetic trap [15] for the first time.

Not only many body systems but also single quantum systems have been an interesting and promising subject of research in quantum optics. Many experiments investigate the detection and manipulation of few or single atoms. The development has improved in such a way that it is nowadays possible to transport single atoms, which are stored in a dipole trap, like being on a conveyor belt [16] or to perform a quantum walk [17] of a single atom.

Different proposals for a combination of a many body system with a single particle and for unbalanced mixtures have been made. For example a single atom being in a superposition state may be cooled by a BEC and therefore gain a much longer coherence time due to the suppression of heating effects [18, 19]. A combination of the two systems allows to use the advantages of both. Single atoms are easy to manipulate but it is difficult to generate coherent interactions between them. In contrast many body systems such as BECs are perfect to study interactions, but single atom resolution remains a challenge. Only recently, single site resolution in optical lattices was demonstrated [20, 21].

In this thesis an experiment using a strongly imbalanced mixture of two bosonic species namely Caesium (^{133}Cs) and Rubidium (^{87}Rb) is investigated. A single Cs atom may serve as a probe for the many particle system, consisting of Rb atoms, causing least possible perturbation. Hence it could be possible to determine phase fluctuations [22] or decoherence [23] of the BEC. First steps to combine the systems were the realisation of a single atom magneto optical trap (MOT) and the construction of a fluorescence detection setup for single atoms [24]. While pervious work[25, 26] was devoted to investigate molecular potentials, the focus is now laid on studies of coherent ground state interactions of a single atom with a many body system.

One of the interesting next aims is to investigate the coherence time of a single atom during the interaction with an ultracold cloud. Therefore, three important requirements have to be fulfilled. First, the single atom needs to be stored in the same optical trap as the ultracold cloud, so that both systems are combined. In a next step one needs to control the internal degree of freedom of the single atom in order to generate a superposition state and in a last step the coherence time of the single atom is studied by Ramsey spectroscopy and spin echo measurements.

My thesis will present the experimental realisation and characterisation of all of these prerequisites necessary for the investigation of the coherence dynamics of single atoms immersed in a quantum gas: In the first chapter, the traps used to combine the single Cs atom with the ultracold Rb cloud are presented and characterised. Afterwards the methods used to control the internal degree of freedom of the Cs atom, e.g. microwave spectroscopy, are introduced. In the last chapter the coherence time of the generated superposition states is measured.

2 Immersion of single Cs atoms into an ultracold Rb gas

The aim of this thesis is to immerse the single Cs atom into the ultracold Rb cloud and to investigate the coherence properties of the single atom. In order to achieve the mixture of both species three different traps are used: a magneto optical trap (MOT), a one dimensional optical lattice and a crossed dipole trap. In this chapter the theory of these different optical traps is introduced. The reason to use three different traps is explained and measurements of characteristic parameters are presented.

The description focusses on the involved traps and the preparation of the single atom, because the preparation of the ultracold cloud has already been discussed in great detail in [25] and [26].

2.1 General overview of the traps involved

All experiments are performed in a glass cell, which is part of an ultra high vacuum system (pressure inside the system 10^{-11} mbar), in order to avoid limitations due to background gas collisions. Figure 2.1 illustrates the three traps used. In the beginning the single Cs atoms are stored in a dissipative magneto optical trap (MOT), whereas the Rb is trapped in a conservative crossed optical dipole trap, from now on referred to as running wave (trap). In order to obtain a high number of Rb atoms in the ultracold cloud, a large trap volume is desired for the running wave trap.

The single atoms trapped in the MOT have a temperature of a few 100 µK, depending on the alignment of the laser beams. As the Rb is evaporatively cooled the running wave trap is very shallow. It is therefore not possible to directly transfer the Cs atoms into running wave trap. Hence, a one dimensional optical lattice, from now on referred to as lattice, is used in an intermediate step. The lattice parameters, e.g. beam waist, wavelength and power, are chosen such that on the one hand a trap depth that allows to store even very hot atoms from the MOT is obtained and on the other hand Rb is only slightly affected by the lattice potential. After transferring the atoms into the lattice, they are further cooled by adiabatic lowering of the lattice potential down to a temperature suitable to store the atoms in the running wave trap. During that process the potential of the running wave trap is still present and in a last step the atoms are

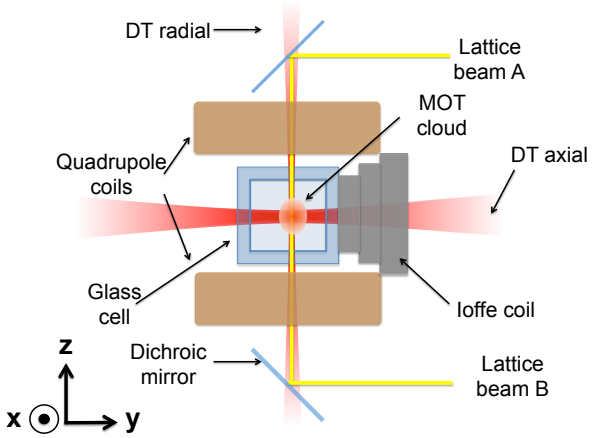

Figure 2.1: Schematic overview on the different traps (not true to scale). Few Cs atoms are trapped in the MOT, which is depicted in orange. The MOT is formed within a glass cell, which contains an ultra high vacuum (UHV). An optical lattice (depicted in yellow) is used in an intermediate step to transfer the Cs atoms into the running wave trap, where the Rb cloud is stored. The lattice is therefore overlapped with the radial beam of the running wave trap (DT radial). The axial beam (DT axial) is shined in perpendicular to the lattice axis. Additionally, quadrupole coils generating the magnetic field for the MOT and the Ioffe coil used to create a magnetic trap for the ultracold cloud are illustrated.

transferred into the running wave trap by lowering the lattice potential to a zero value.

2.2 Magneto optical trap for single Cs atoms

A magneto optical trap (MOT) uses the technique of laser cooling to cool single atoms [1, 27]. The atoms are cooled by six perpendicular and counter propagating laser beams. The laser beams are red detuned, which together with the Doppler effect causes the atoms to preferably absorb *counterpropagating* photons. In this process, the atom is given a momentum kick in direction of the photon before absorption. The atom is deexcited by the spontaneous emission of a photon and because the direction of spontaneous emission is isotropic, the atoms are cooled by the momentum exchange and pushed towards the centre of the cooling region.

With this method the atoms are cooled but not trapped to the region of interest. Therefore quadrupole coils are used to generate a magnetic field, which increases with radial distance to the cooling region. Because of Zeeman splitting, which is proportional to the magnetic field, the atoms experience a position-depending force towards the cooling region. The polarisation of the laser beams determines the direction in which the atom

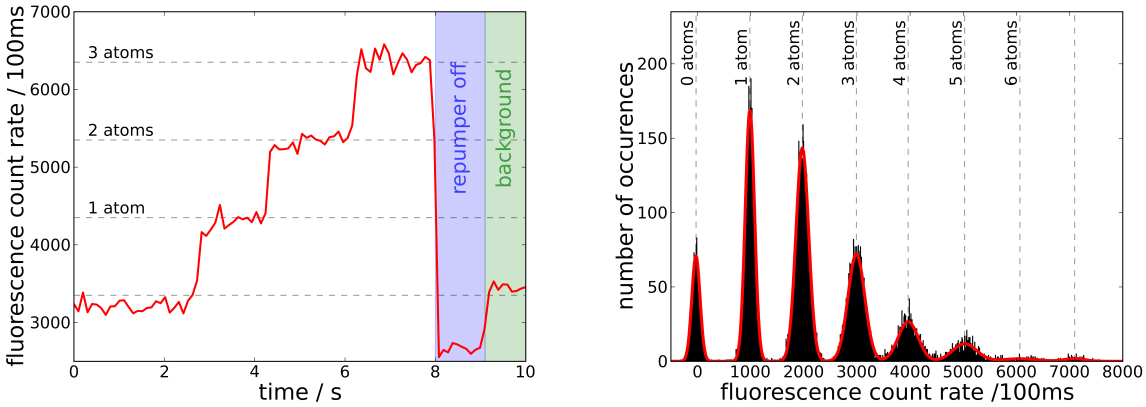

Figure 2.2: In the figure on the left, a loading curve of the MOT in high gradient phase is shown. One can see that only one atom per second is loaded into the MOT. The right picture illustrates a typical histogram recorded for the Cs MOT with fluorescence imaging. The fluorescence count rate is related to the number of atoms in the trap. Each gaussian distribution of fluorescence counts belongs to a specific atom number. Each distribution is well separated from its nearest neighbours, enabling a good resolution when counting the number of atoms. In addition the histogram reveals that during the MOT loading phase only up to 5 atoms are trapped. [Pictures: N.Spethmann]

is pushed. Therefore laser beams with opposite handed circular polarisation are used (σ^+ and σ^- light).

In this experiment the hyperfine states $|F = 4\rangle$ and $|F' = 5\rangle$ of the Cs atom are used as the cooling cycling transition, which leads to a wavelength of 852 nm for the cooling laser. Due to a finite excitation probability into the $|F' = 4\rangle$ level, the atom may decay into the $|F = 3\rangle$ state and hence no longer participates in the cooling cycle. In order to correct this another laser - the repumping laser - is used to transfer the atoms back into the $|F' = 4\rangle$ state.

There are some possibilities to tune the MOT to only trap single Cs atoms, which is desired in our experiments. At the beginning of the loading phase, a low magnetic field gradient of 60 G/cm is used for 150 ms to load few atoms into the MOT. Then the magnetic field is increased to about 300 G/cm. With this method and with small MOT beam diameters, the trapping region is held small and therefore a loading rate of about 1 atom/s is achieved. In picture 2.2 a typical trace of the high gradient MOT phase is shown.

The atoms are detected by a sensitive fluorescence imaging system which was built in a prior Diploma thesis [24]. It consists of an high numerical aperture objective and

a single photon counting module (SPCM). By illuminating the atoms in the MOT with near resonant light, they send out fluorescence photons which are collected by the objective an guided through a glass fibre onto the SPCM chip. The chip is sensitive to single photons and from the count rate of the chip it is possible to derive the atom number. A recorded histogram, which is shown in figure 2.2(right), reveals the relation between the fluorescence count rate and the atom number. Typical values for one atom are about 800-1000 counts/100 ms depending on the alignment of the MOT position with respect to the imaging system as well as on parameters of the laser beams.

2.3 Optical Lattice

Because of the high temperature of the atoms in the MOT and its dissipative character, it is not possible to directly transfer the atoms into the very shallow potential of the running wave trap. Hence a one dimensional optical lattice is used to further cool the atoms and to transfer them into the running wave trap. Furthermore the lattice is also used to recapture the atoms from the running wave trap and reload them into the MOT, where the atoms can be detected again. This is an important step because all our experiments rely on counting the atom number before and after manipulation of the atoms.

2.3.1 Theoretical description

The optical lattice is formed out of two linear polarised counter propagating gaussian laser beams. Due to the interaction of the red detuned laser beams with the dipole moment of the atom, a row of harmonic potential wells are formed. The distance between these potentials is given by the periodicity of the standing wave ($= \lambda_{\mathrm{opt}}/2$).

The optical lattice is a quantum mechanical effect but nevertheless it may be described by a classical model. The lattice is comparable to the Lorentz model of a classical damped harmonic oscillator which is driven by an external electric field [28, 29]:

$$\mathbf{E}(\mathbf{r},t) = (\mathbf{E}_0(\mathbf{r})\exp(-i\omega t) + c.c.)/2\,. \tag{2.1}$$

In this model the dipole moment of the atom fulfils the classical equation of motion

$$\ddot{\mathbf{d}}(\mathbf{r},t) + \Gamma_\omega \dot{\mathbf{d}}(\mathbf{r},t) + \omega_0^2 \mathbf{d}(\mathbf{r},t) = \frac{e^2}{m_e}\mathbf{E}(\mathbf{r},t)\,, \tag{2.2}$$

with ω_0 the resonance frequency of the oscillator and Γ_ω the damping rate due to the classical dipole radiation

$$\Gamma_\omega = \frac{e^2\omega^2}{6\pi\epsilon_0 m_e c^3} \tag{2.3}$$

with m_e the rest mass and e the charge of the electron and ϵ_0 the dielectric constant. The induced dipole moment is related to the electric field via the complex polarisability $\alpha(\omega)$:

$$\mathbf{d}(\mathbf{r},t) = \alpha(\omega)\mathbf{E}(\mathbf{r},t)\,. \tag{2.4}$$

The stationary solution of equation (2.2) leads to

$$\alpha(\omega) = \frac{e^2}{m_e}\frac{1}{\omega^2-\omega_0^2-i\omega\Gamma_\omega} = \frac{6\pi\epsilon_0 c^3(\Gamma_{\omega_0}/\omega_0^2)}{\omega^2-\omega_0^2-i\omega^3(\Gamma_{\omega_0}/\omega_0^2)}\,. \tag{2.5}$$

In the last step the on-resonance damping rate $\Gamma_{\omega_0} = (\omega/\omega_0)^2\Gamma_\omega$ and equation (2.3) were used. The time average of the interaction energy between the induced dipole moment and the driving electric field leads to the dipole potential

$$U_{\mathrm{dip}}(\mathbf{r}) = -\frac{1}{2}\langle\mathbf{d}(\mathbf{r},t)\mathbf{E}(\mathbf{r},t)\rangle = -\frac{1}{2\epsilon_0 c}\,\mathrm{Re}\,\alpha(\omega)I(\mathbf{r})\,, \tag{2.6}$$

which depends on the field intensity $I(\mathbf{r}) = c\epsilon_0|\mathbf{E}_0(\mathbf{r})|^2/2$ and the real part of the polarisability.

In a dipole trap the atom scatters photons from the trap laser, which is described by the photon scattering rate

$$R_s(\mathbf{r}) = \frac{\mathrm{P}_{\mathrm{abs}}(\mathbf{r})}{\hbar\omega} = \frac{1}{\hbar\omega}\langle\dot{\mathbf{d}}(\mathbf{r},t)\mathbf{E}(\mathbf{r},t)\rangle = \frac{1}{\hbar\epsilon_0 c}\,\mathrm{Im}\,\alpha(\omega)I(\mathbf{r})\,, \tag{2.7}$$

which is derived similarly to the dipole potential by using the absorbed power P_{abs}.

In this experiment, the rotating wave approximation can be used because the detuning of the laser $\Delta = \omega - \omega_0$ is much larger than the natural line width Γ. Additionally the detuning is much smaller than the resonance frequency ω_0 ($|\Delta| \ll \omega_0$) and therefore $\omega/\omega_0 \approx 1$. It is now possible to write equations (2.6) and (2.9) as

$$U_{\mathrm{dip}}(\mathbf{r}) = \frac{3\pi c^2}{2\omega_0^3}\frac{\Gamma}{\Delta}I(\mathbf{r})\,, \tag{2.8}$$

$$R_s(\mathbf{r}) = \frac{3\pi c^2}{2\hbar\omega_0^3}\frac{\Gamma^2}{\Delta^2}I(\mathbf{r})\,. \tag{2.9}$$

One can see that both parameters depend linearly on the field intensity. The potential U_{dip} scales linearly with $1/\Delta$ whereas the photon scattering rate scales quadratically with it. Hence R_s decreases by increasing the detuning but this also leads to a lower potential depth. This effect is compensated with increasing the field intensity. Furthermore, equation (2.8) demonstrates that the force depends on the sign of the detuning.

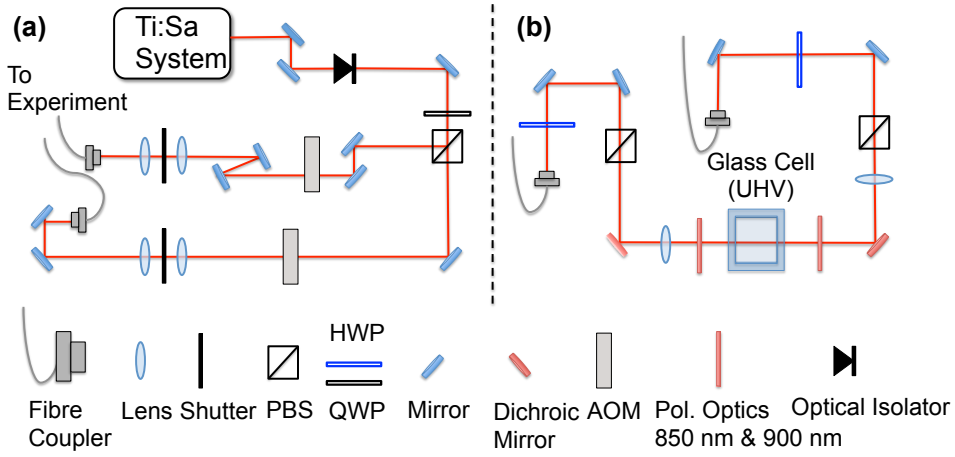

Figure 2.3: (Figure not true to scale.)**(a)** Schematic sketch of the optical setup for the lattice before the light is guided to the experimental table. The laser light is generated by a Ti:Sa system. It passes first an optical isolator and is then splitted into two different beams by use of a quarter wave plate (QWP) and a polarising beam splitter cube (PBS). With an acousto-optic modulator (AOM) the power of each beam, which is transmitted via single-mode-polarisation-maintaining-fibres to the main experimental table, is stabilised. A telescope is used to focus the beam in order to achieve a high coupling efficiency into the fibre. **(b)** Setup for the lattice on the experimental table. The polarisation of the beams is increased by use of a half wave plate (HWP) and a PBS. With dichroic mirrors the beams are coupled into the glass cell and a lens focusses the beams down to 31 µm at the position of the atoms.

The trap frequencies, which are the oscillation frequencies of the atom in the trap, in axial and radial direction are given by

$$\omega_{\mathrm{rad}} = \left(\frac{4U_0}{mw_0^2}\right)^{1/2} \tag{2.10}$$

$$\omega_{\mathrm{ax}} = \left(\frac{2U_0}{mz_0^2}\right)^{1/2} . \tag{2.11}$$

Here w_0 denotes the beam waist and z_0 the Rayleigh length of the beam described in Gaussian optics (details on Gaussian optics can be found in [30]).

2.3.2 Experimental Setup

In order to generate the lattice potential a commercially available Titanium:sapphire (Ti:Sa) laser (Model: Microlase MBR-110) was aligned during this thesis. It is pumped by a frequency doubled Neodym:YAG laser (Spectra Physics MilleniaX) which delivers a power of 10 W at a wavelength of 532 nm. This leads to an output power of 700

mW for the Ti:Sa laser operating at a wavelength of 899.9 nm. The wavelength differs by only 5.3 nm from the Cs D_1 line [31] leading to a photon scattering rate of a few 100 Hz, which is the limiting factor for the longitudinal relaxation time T_1 (see sec. 4.2). However, the chosen wavelength provides the desired trap depth for the Cs atoms and at the same time does not disturb the Rb. For more details on this point see [24, 32].

A schematic view on the optical path, which was set up during the thesis is shown in figure 2.3. After passing an optical isolator (Newport) the laser beam is divided into two beams, each containing roughly half of the laser power. In using a setup consisting of a half wave plate (HP) and a polarising beam splitter cube (PBS) one is able to change the power distribution of the beams. With acousto-optic modulators (AOM) the power is actively stabilised and controlled by an electronical feedback loop. By means of single-mode-polarisation-maintaining-fibres the light is guided to the vacuum setup and is coupled into the vacuum chamber via dichroic mirrors, which transmit light of 860 nm and lower but are reflective for wavelengths greater than 860 nm. Afterwards the light passes a lens to focus the beam to a waist of $w_0 = 31\,\mu\text{m}$ at the position of the atoms. After passing all optical components, a maximum laser power of 150 mW in each beam is achieved.

To be sure that both beams perfectly overlap, one beam was coupled into the fibre output of the other beam. In this case a coupling efficiency of 65% from one fibre into the other is achieved. The deviation from unity arises due to aberration caused by the optical elements in the beam path (see fig. 2.3) which affects the coupling efficiency.

2.3.3 Transfer efficiency and lifetime measurement

With the current experimental setup it is only possible to detect the Cs atoms during MOT phases. Because nearly all performed experiments rely on the atom number statistics before and after manipulation of the atoms, it is crucial to have a good transfer efficiency between both traps. Hence, the alignment of the traps is an important step. To gain the maximal overlap of MOT and lattice, the light shift caused by the AC-Stark effect is used [33]. At the position of maximum observed light shift, the atoms see the maximum intensity of the lattice beams and best alignment is achieved. We therefore move the position of the lattice and directly study the light shift on the atoms stored in the MOT, visible as a loss of fluorescence counts due to a shift of the resonance frequency. Figure 2.4 shows a typical trace observed at best position of the lattice. After the alignment of the traps a lifetime measurement for the atoms stored in the lattice is performed, which also reveals the transfer efficiency.

In order to investigate the lifetime, first atoms are loaded into the MOT and held there for about 150 ms to count the atom number. Afterwards the lattice is switched on and both traps are operated at the same time for 50 ms. To transfer the atoms into

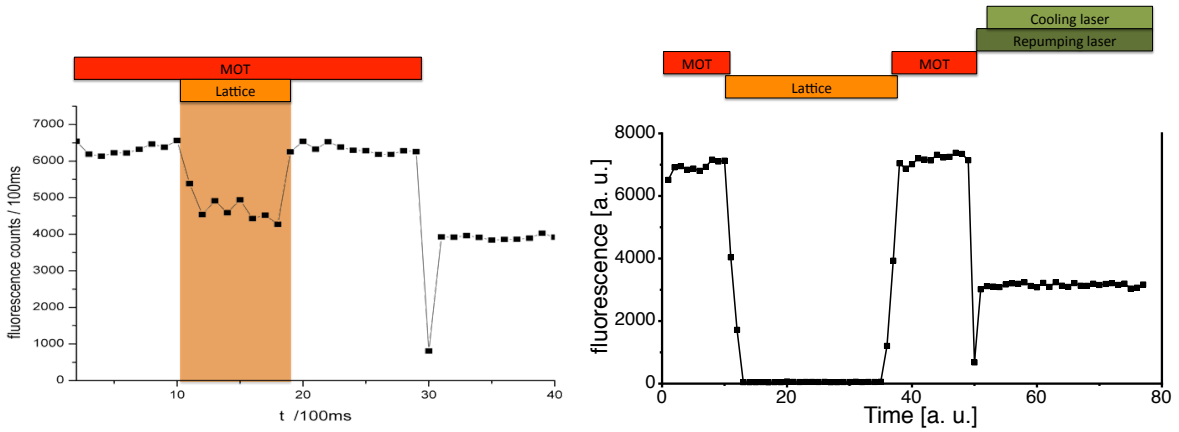

Figure 2.4: (Left) A typical trace for observing the light shift is shown. The MOT and the lattice are operated at the same time and due to the light shift caused by the lattice, leading to a slightly different resonance frequency of the atoms, a loss of fluorescence counts is observed. **(Right)** This picture illustrates the sequence to measure the lifetime of the atoms: During the MOT phases the captured atoms are illuminated by near resonant light to determine the number of atoms with fluorescence imaging. In a next step atoms are transferred to and stored in the lattice for a certain amount of time. In the lattice no fluorescence is observed due to the off-resonant wavelength of the lattice laser. Afterwards the atoms are reloaded into the MOT and their number is determined again. From the difference of atom numbers before and after the sequence for different storage times in the lattice, the lifetime can be extracted. At the end of every experimental cycle the background photons from the MOT lasers are detected.

the lattice, the MOT lasers are switched off before the quadrupole field is shut down. This process was optimised in order to obtain the best transfer efficiency. Afterwards the atoms are trapped only in the lattice potential for a certain time period in which the experiments are performed. The same temporal overlap between the MOT and the lattice is used during the reload of atoms back into the MOT potential. Here the atom number is counted again. This experimental cycle is repeated 100 times with 2 atoms in average to obtain a desired statistical error less than 3%. During the whole thesis this experimental cycle is the standard technique (unless stated differently) and only enhancements will be explained.

Comparison of the survival probability with the different holding times in the lattice leads to the parameters of lifetime and transfer efficiency. Figure 2.5 shows the measured data points for the survival probability versus the holding time in the lattice as well as the used fit function $p(t) = p_0 \exp(t/\tau)$. In this function the parameter p_0 denotes the achieved transfer efficiency between the MOT and the lattice. From the fit one obtains an efficiency of $p_0 = 1.06 \pm 0.07$. The transfer efficiency is over estimated

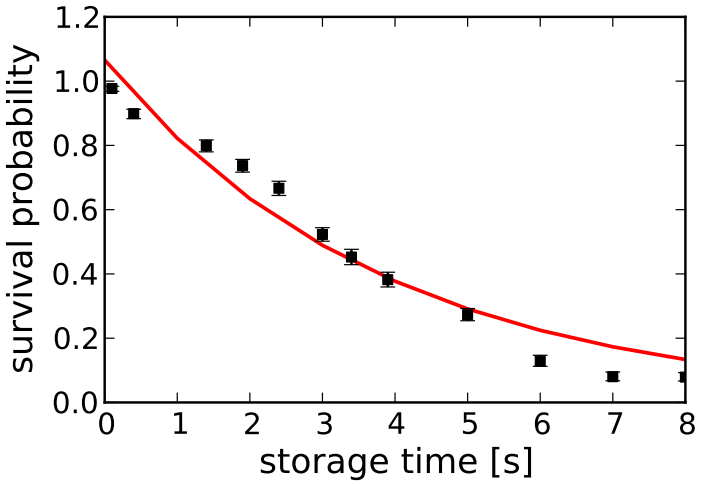

Figure 2.5: Survival probability of the atoms versus the storage time in the lattice. The red solid line indicates the fit function (see text).

in this case, due to the fact that the measured data points do not exactly follow an exponential decay. However, a transfer efficiency close to unity is achieved. The lifetime of the atoms is given by τ which is inferred from the fit to be $\tau = 3.9 \pm 0.3$ s. The limiting factor in this case is as recoil heating. As the laser wavelength of 899.9 nm is close to the resonance wavelength of 894 nm, it causes a photon scattering rate in the order of a few 100 Hz at maximum beam power. This benefits recoil heating due to spontaneous photon scattering. Laser intensity fluctuations are estimated to maximum 0.5% of the initial laser intensity and therefore are too small to affect the lifetime. Collisions between atoms placed in the lattice are suppressed due to the low atom number and their separation by many potential wells. Collisions with the background gas are also very unlikely, because a lifetime of 160 s for Rb in the magnetic trap was observed.

2.3.4 Trap frequencies

As a next step the oscillation frequency of the atom in the lattice is measured. This is done in both axial and radial direction of the trap. The sequence is similar to that of the lifetime measurement. After loading the atoms into the lattice, the laser intensity is modulated with a sinusoidal waveform, of frequency ω_{mod}. During the stepwise scanning of the modulation frequency, which is done with a combination of a signal generator and the AOMs placed in the beam path, it crosses the resonance of the atoms. This results in heating and hence the escape of atoms from the trap. The trap is adiabatically lowered to a trap depth where approximately 70% of the atoms survive in order to observe the loss of atoms for small modulations of the potential. Here a modulation time of 200 ms with a modulation of $\pm 10\%$ of the trap depth ensures a significant parametric excitation. Adiabatically lowering the trap depth to about 10% of its initial value leads

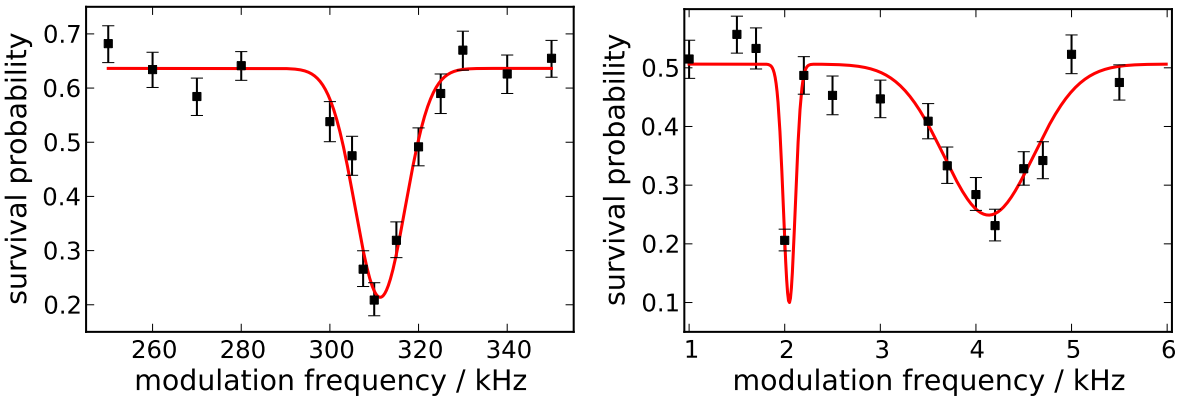

Figure 2.6: Shown is the survival probability versus the excitation frequency. The loss of atoms occurs due to heating at the resonance frequency. The red solid line indicates the function fitted to the data (see text).

to a significant loss of atoms. Figure 2.6 shows the observed spectra of both beams. An exponential function of $p(\omega_{\mathrm{mod}}) = p_0 \exp(-\omega_{\mathrm{mod}}/b)$ fitted to the data reveals the parametric excitation frequency. Due to its good confinement in axial direction, leading to a high oscillation frequency, the strongest loss of atoms at a frequency of $\omega_{\mathrm{mod}} = 311\,\mathrm{kHz}$ is observed. This agrees well with the theoretically expected value of $\omega_{\mathrm{ax,calc.}} = 362\,\mathrm{kHz}$ for the axial trap frequency. However, the dip does not show parametric but resonant heating. This might occur because of the used electronic setup: As the PID controller of the AOM has a bandwidth, which is too small to be used at such high frequencies, a small additional electric setup was placed behind the controller. Due to this setup higher harmonics of the electronic signal might be generated and therefore a dip at the resonance frequency instead of a dip at parametric frequency is observed. As no other dips are observed at lower as well as at higher frequencies, we conclude that this is the resonant frequency.

In radial direction, where the confinement is much weaker, one observe a loss of atoms at $\omega_{\mathrm{mod}} = 4.2\,\mathrm{kHz}$ and at $\omega_{\mathrm{mod}} = 2.1\,\mathrm{kHz}$ corresponding to parametric and resonant heating, respectively. This leads to a trap frequency of $\omega_{\mathrm{rad}} = 2.1\,\mathrm{kHz}$. This fits within 90% to the calculated value of $\omega_{\mathrm{rad,calc.}} = 2.4\,\mathrm{kHz}$ [34].
The good agreement of the expected and measured parameters reveals that the lattice is build in such a way that it fulfils the theoretically expected parameters such as the beam waist and the trap depth.

2.4 Temperature measurements in the lattice

Knowing all parameters of the trap, a temperature measurement in the lattice is performed. There are many different ways to measure the temperature of an atom ensemble

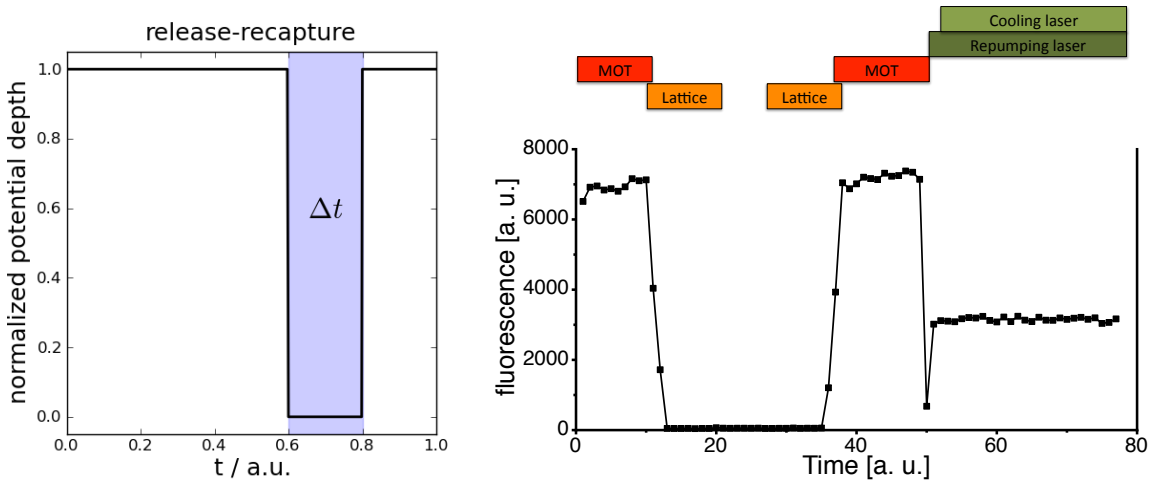

Figure 2.7: (Left) The trap potential is switched off for a waiting time Δt and the atoms escape the trap. Afterwards the trap is ramped up again to recapture remaining atoms. **(Right)** Sequence used for the release recapture measurements. After the atom number in the MOT has been counted, atoms are transferred into the lattice, where they are stored for a short time. The lattice potential is switched off for a waiting time Δt and then switched on again. The atoms are recaptured in the lattice and reloaded into the MOT, where the atom number is obtained by fluorescence imaging.

like time of flight measurements, adiabatic lowering [33] or release recapture measurements [35]. From this methods only adiabatic lowering and release recapture are suitable for single atoms and both are used here to investigate the temperature of the single atoms in the lattice. The difference between both methods is that adiabatic lowering reveals the thermal distribution of the atoms, whereas the thermal distribution must be known or estimated for the release recapture method. From the release recapture technique a more precise value at low temperatures (in the regime of a few µK) is obtained and therefore it is the preferred method throughout this thesis.

2.4.1 Release recapture method

The method of release recapture is a standard and easy-to-perform technique to measure the temperature of single atoms, which is used in many experiments [35]. It takes advantage of the thermal velocity distribution of the atoms. After atoms are trapped, the potential is switched off rapidly and the atoms are released. For a short time Δt the trapping potential remains out of use. The hot atoms escape from the trap volume, while colder and therefore slower atoms stay in the trap region. By switching on the trap again the latter ones are recaptured into the potential. The relation between the velocity distribution of the atoms and the waiting time determines the fraction of surviving atoms. A schematic drawing of this principle is shown in figure 2.7(left). Temperature

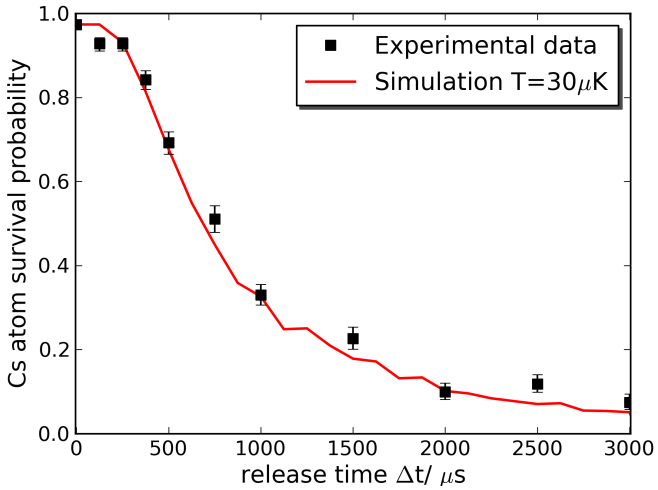

Figure 2.8: The survival probability is plotted as a function of the release time. Also shown are the numerically calculated graphs [36]. The red solid line denotes the simulated graph with the trend fitting best to the measured data, whereas the dashed lines are shown to illustrate the significance of the fit.

is an ensemble parameter and hence, many iterations per Δt with only few atoms in the lattice are performed.

2.4.2 Experimental results

Again a similar experimental cycle as explained in section 2.3.3 is performed with the only difference, that the lattice potential is completely switched off for the release time (see fig. 2.7). The shut down process of the lattice is performed diabatically to avoid adiabatic cooling. These measurements were carried out for release times from 0 µs up to 3 ms. Figure 2.8 shows the measured survival probability as a function of the release time Δt. The curves to the corresponding temperatures are calculated numerically (for details on the calculations see [36]). The red solid line is the curve which is in best agreement to the trend of the data points. Whereas the dashed lines indicate upper and lower bounds for the temperature. In this case the curve in best agreement with the data points leads to a temperature of the atoms in the lattice of about 30 µK. Comparable results were obtained in similar setups used by other members of this group, although temperatures were obtained with the adiabatic lowering technique [33].

2.5 Atoms in the running wave trap

In the last section the transfer of the single atom into the lattice was explained and a transfer efficiency close to unity was achieved. The last step is therefore to combine the

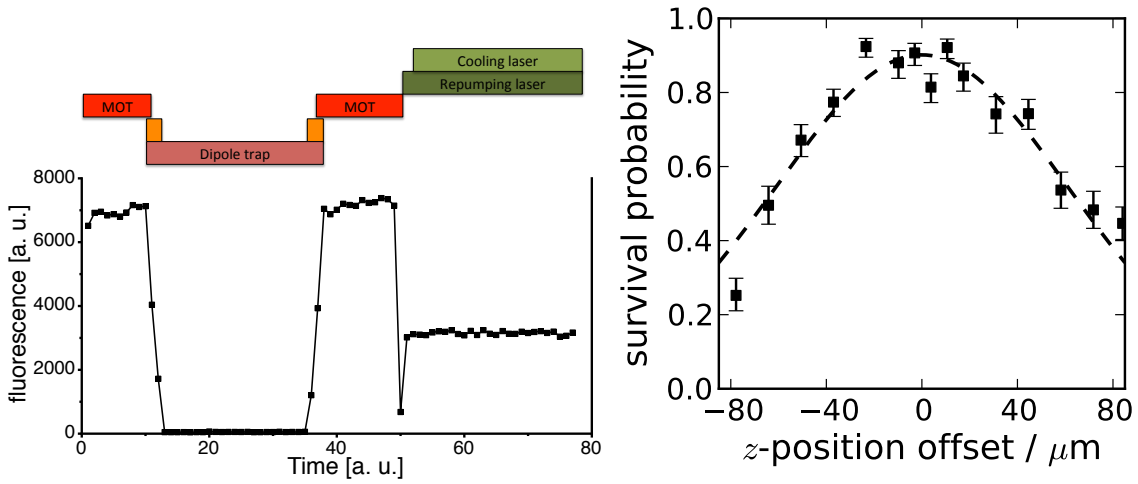

Figure 2.9: (Left) Sequence used to transfer the atom into the running wave trap. The process remains the same for the MOT and the lattice, except that during the lattice phase the running wave trap potential is already present. With adiabatic lowering of the lattice, which cools the atoms, the transfer into the running wave trap takes place. **(Right)** Survival probability of the Cs atoms loaded into the running wave trap versus the position offset of the axial beam in z direction

single Cs atom and the ultracold cloud in the running wave trap.

2.5.1 Experimental setup

Two perpendicular aligned laser beams form the optical dipole trap, generated by a fibre amplifier system at 1064 nm. It consist of a seed laser (CrystaLaser) with a power of a few 100 mW and a fibre amplifier (Nufern Laser) delivering a power of 10 W. With a polarising beam splitter cube and a half wave plate, allowing a variable power splitting, the power is divided into two beams. Both beams pass a shutter and an AOM, which is used to control the beam power, before the beams are guided via a special glass fibre for high light intensities (Liekki) to the experimental table (Details on this setup see [26]). One beam, called axial beam (see fig. 2.1, is focussed through the Ioffe coil, which is part of the QUIC trap [37] to generate the ultracold cloud (see [25, 26]), and has a beam waist of 100 µm. Using a dichroic mirror the radial beam is coupled onto the same axis as the lattice and is focussed down to a beam waist of 48 µm. This ensures high spatial overlap of the beam with the lattice and thus a high transfer efficiency. In the experiments we use a power of 2 W in the axial direction and a power of 0.6 W in radial direction (unless stated differently). With the mentioned parameters we obtain a trap depth of $\approx 100\,\mu K$ for the Cs atoms in the dipole trap.

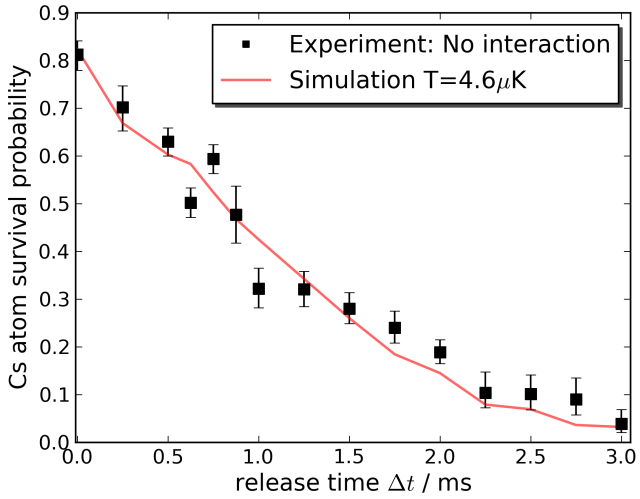

Figure 2.10: Survival probability versus release time in the running wave trap. The black squares are the measured data points and the red solid line indicates the simulated graph with the trend fitting best to the measured data.

2.5.2 Transfer and temperature measurement of single atoms in the running wave trap

A crucial step during the sequence is to transfer the atoms from the lattice into the running wave trap. Hence, a good spatial overlap of both traps is needed to avoid atom losses. As already mentioned in the last section, the lattice and the radial beam of the dipole trap are operated on the same experimental axis, which allows to couple the dipole trap beam into the fibre of one lattice beam (see fig. 2.3 and fig. 2.1), which results in a good spatial overlap of both beams. Because the lattice is well aligned with respect to the MOT, overlapping one beam of the running wave trap with the lattice simultaneously guarantees a well aligned overlap of the running wave with the MOT.

For the axial beam of the trap, a measurement was performed to find the best position, which is defined as the position where the maximal transfer efficiency for the Cs atoms occurs. The transfer efficiency was measured at different voltages of a piezo electric mirror, resulting in slightly different positions in z direction of the dipole trap (see fig. 2.9).

The experimental sequence is performed as follows (see also fig. 2.9):

1. A few atoms are stored in the lattice and at the same time the running wave trap is ramped up to its full power.

2. Then the lattice is adiabatically lowered within a few ms leading to further cooling

of the atoms.

3. At a certain lattice depth, the Cs atoms leave the trap and are from now on stored in the crossed dipole trap.

At the point of best alignment a transfer efficiency of $\approx 93\%$ is achieved. With the already explained technique of a release recapture, one experimentally measures a temperature of $4.6\,\mu K$ for the single atoms in the running wave trap (see fig 2.10). The lower temperature occurs due to the adiabatic lowering of the lattice, which results in cooling of the single atom. For more details on the transfer of Cs atoms, when Rb in the running wave is present, see [34].

3 Coherent control of the internal degree of freedom of a single Cs Atom

In the previous chapter, the experimental procedure to store the single Cs atom in the same trap as the ultracold Rb cloud was discussed. The next step is to investigate the coherence time of the single atom. Therefore it is necessary to control its internal degree of freedom. This is only possible in the lattice or the running wave trap, because of their conservative and state preservative potential.

The desired state for the Cs atom is the $|F = 3, m_{\mathrm{f}} = 3\rangle$ state, which is the absolute ground state so that no decay channels for Cs-Rb collisions exist (Note that Cs-Rb-Rb collisions are still possible). Optical pumping [38, 39] is used to prepare the atoms in the desired state $|3, 3\rangle$.

In order to generate a superposition state, of which the coherence time is investigated, the transition between $|3, 3\rangle$ and $|4, 2\rangle$ is driven by a microwave pulse. The $|4, 2\rangle$ state is chosen, because it provides the longest coherence time in combination with the $|3, 3\rangle$ state. This is required if one wants to investigate the cooling of the superposition state, where the thermalisation time is in the order of 25 ms [36]. By the use of methods such as microwave spectroscopy and driven Rabi oscillations, the control parameters for the internal degree of freedom are studied.

The interaction between the single atom and the microwave radiation field and its dynamical evolution is to good approximation described by the semiclassical Bloch vector model. In this model the classically treated radiation field interacts with a quantum mechanical two level atom.

A variant of the Bloch equations [40], namely the optical Bloch equations are a system of three differential equations. They delineate the evolution of the Bloch vector on the Bloch sphere, which is comparable to the dynamical evolution of a spin-1/2 system in presence of a magnetic field. Here the dynamical evolution of a pseudo spin system with the atomic polarisation and the population difference as the components of the vector is used instead. In the next chapters the Bloch vector model is extensively used

to describe the experimental processes.

3.1 Optical Bloch equations

In this section the optical Bloch equations, which define the evolution of a pseudo spin vector in an magnetic field, will briefly derived (for details see [41, 42]). The Hamilton operator of a two level atom with ground state $|g\rangle$ and excited state $|e\rangle$ reads

$$\hat{H}_{\mathrm{A}} = \frac{\hat{p_{\mathrm{A}}}^2}{2m} + \frac{\hbar\omega_0}{2}(|e\rangle\langle e| - |g\rangle\langle g|), \tag{3.1}$$

with m the mass of the atom and ω_0 the transition frequency between $|e\rangle$ and $|g\rangle$. For the interaction of the atom with an external electromagnetic field $\mathcal{E}$ the dipole potential can be expressed as

$$V_{\mathrm{dip}} = -\hat{d}\mathcal{E} \tag{3.2}$$

where $\hat{d}$ denotes the dipole moment operator. In the case of atoms, a permanent dipole moment does not exist and this leads to

$$\begin{aligned} \hat{d}_{eg} &= -e\hat{r}_{eg} = \langle e|\hat{d}|g\rangle & (3.3)\\ \hat{d}_{eg} &= d_{eg}\langle e|g\rangle + d_{ge}\langle g|e\rangle \\ &= d_{eg}\hat{\sigma}^\dagger + d_{ge}\hat{\sigma}. & (3.4) \end{aligned}$$

By using these expressions and the relation $\hat{\sigma}^\dagger\hat{\sigma} = |e\rangle\langle g|g\rangle\langle e| = |e\rangle\langle e|$ the Hamilton operator and the dipole potential can be rewritten as

$$\begin{aligned} \hat{H}_{\mathrm{A}} &= \frac{\hat{P_{\mathrm{A}}}^2}{2m} + \hbar\omega(\hat{\sigma}^\dagger\hat{\sigma} - 1/2) & (3.5)\\ \hat{V}_{\mathrm{dip}} &= -(d_{eg}\hat{\sigma}^\dagger + d_{ge}\hat{\sigma})\mathcal{E}_0\cos(\omega t). & (3.6) \end{aligned}$$

It is now possible to express $\hat{\sigma}^\dagger$ and $\hat{\sigma}$ in terms of the Pauli matrices $\hat{\sigma}_x, \hat{\sigma}_y, \hat{\sigma}_z$

$$\hat{\sigma}^\dagger = \frac{1}{2}(\hat{\sigma}_x + i\hat{\sigma}_y) \qquad \hat{\sigma} = \frac{1}{2}(\hat{\sigma}_x - i\hat{\sigma}_y) \tag{3.7}$$

and this leads to the final expressions for $\hat{H}_{\mathrm{A}}$ and $\hat{V}_{\mathrm{dip}}$

$$\begin{aligned} \hat{H}_{\mathrm{A}} &= \frac{\hat{P_{\mathrm{A}}}^2}{2m} + \frac{\hbar\omega_0}{2}\hat{\sigma}_z, & (3.8)\\ \hat{V}_{\mathrm{dip}} &= -d_{eg}\mathcal{E}_0\cos(\omega t)\hat{\sigma}_z\,. & (3.9) \end{aligned}$$

The solutions of the equation of motion for the Pauli operators written in the Heisenberg picture

$$\dot{\hat{\sigma}}_j = \frac{i}{\hbar}[\hat{H}_{\mathrm{A}} + \hat{V}_{\mathrm{dip}}, \hat{\sigma}_j] \tag{3.10}$$

lead to the set of equations

$$\dot{\hat{\sigma}}_x = -\omega_0 \hat{\sigma}_y \tag{3.11}$$

$$\dot{\hat{\sigma}}_y = \omega_0 \hat{\sigma}_x - \frac{2 d_{eg} \mathcal{E}_0}{\hbar} \cos(\omega t) \hat{\sigma}_z \tag{3.12}$$

$$\dot{\hat{\sigma}}_z = \frac{2 d_{eg} \mathcal{E}_0}{\hbar} \cos(\omega t) \hat{\sigma}_y \, . \tag{3.13}$$

Note that here the Pauli matrix operators describe only a pseudo-spin system.

In absence of a driving field, i.e. $\mathcal{E}_0 = 0$, the system rotates rapidly around the z-axis. By introduction of the frequency ω_D of the driving field and by transformation into a frame rotating at $\omega = \omega_D$ the rapid rotation is eliminated.

In the semi classical treatment, which is valid at high microwave power, the expectation values of the Pauli matrix operators are written like

$$\langle \hat{\sigma}_x \rangle = u \cos(\omega t) - v \sin(\omega t) \tag{3.14}$$

$$\langle \hat{\sigma}_y \rangle = u \sin(\omega t) + v \cos(\omega t) \tag{3.15}$$

$$\langle \hat{\sigma}_z \rangle = w \tag{3.16}$$

with

$$\dot{u} = \delta v + \Omega_R \sin(2\omega t) w \tag{3.17}$$

$$\dot{v} = -\delta v + \Omega_R (1 + \cos(2\omega t)) w \tag{3.18}$$

$$\dot{w} = -\Omega_R \sin(2\omega t) u - \Omega_R (1 + \cos(2\omega t)) v \, . \tag{3.19}$$

Here the Rabi frequency $\Omega_R = d_{eg} \mathcal{E}_0 / \hbar$ and the detuning $\delta = \omega - \omega_0$ from the atomic resonance have been introduced.

In the rotating wave approximation ($|\delta| \ll \omega_0$) terms containing 2ω can be neglected due to fast rotation. Applying this to equations (3.17-3.19) leads to the so called optical Bloch equations:

$$\dot{u} = \delta v \tag{3.20}$$

$$\dot{v} = -\delta v + \Omega_R w \tag{3.21}$$

$$\dot{w} = -\Omega_R v \, . \tag{3.22}$$

Note that these equations do not include damping. The damped Bloch equations are introduced later. It is also possible to write the Bloch equations in a single vector equation

$$\dot{\mathbf{u}} = -\boldsymbol{\Omega} \times \mathbf{u} \tag{3.23}$$

with the torque vector $\mathbf{\Omega} = (\Omega_R, 0, 0)$ and the so called Bloch vector $\mathbf{u} = (u, v, w)$. In case of the undamped Bloch equations the Bloch vector has unit length and its evolution lies on a unit sphere. A magnetic dipole transition is to good approximation described by the Bloch equations. In this case the u and v components of the Bloch vector delineate the components of the magnetic dipole moment which are in phase and in quadrature with the driving field $\mathcal{E}$, respectively. Furthermore equation (3.22) infers that u is the dispersive component of the dipole moment and v is the absorptive component. The population number difference of the two states is given by w and only one state is populated in case of $w = \pm 1$.

It is also possible two write the Bloch vector in other representations of the two level atom. A very common one is the state vector representation. The derivation of the transformation into the corresponding state vector is not shown here (see [42]) but the very descriptive solution is presented:

$$u = \sin\vartheta \cos\phi \tag{3.24}$$
$$v = \sin\vartheta \sin\phi \tag{3.25}$$
$$w = \cos\vartheta\,. \tag{3.26}$$

Here ϑ describes the angle of the Bloch vector with the w-axis and ϕ describes its position in the uv-plane.

3.1.1 Rabi oscillations and resonant pulses

Rabi oscillations

In most cases it is not possible to solve the Bloch equations analytically, but some special cases exist (see figure 3.1). The solution for an atom in a coherent radiation field leads to an oscillation between the ground and excited state. With initial values of the Bloch vector of $\mathbf{u} = (0, 0, -1)$ and a detuning of δ from the resonance frequency, the time evolution is given by [42]

$$w(t, \delta) = -1 + \frac{2\Omega_R^2}{\Omega^2} \sin^2(\frac{\Omega t}{2}) \tag{3.27}$$

where

$$\Omega = \sqrt{\delta^2 + \Omega_R^2} \tag{3.28}$$

is the generalised Rabi frequency. It denotes the frequency with which the atom flips between both states. Equation (3.27) demonstrates that complete population transfer is only possible in case of $\delta = 0$, which leads to the simple form

$$w(t, \delta = 0) = -\cos(\Omega_R t) \tag{3.29}$$

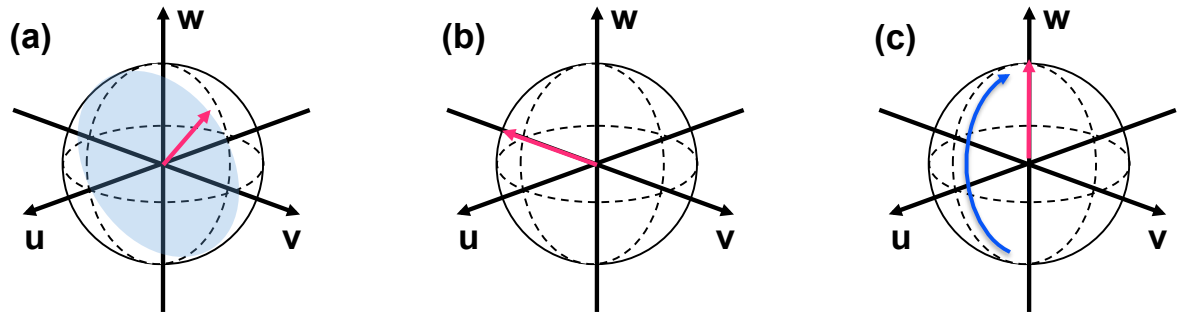

Figure 3.1: Rotation of the Bloch vector **u** on the Bloch sphere. Picture **(a)** shows a rotation of the Bloch vector about the u axis for a resonant pulse. The flipping into the uv plane for a $\pi/2$ pulse is illustrated in **(b)** and **(c)** delineates the total population transfer corresponding to a complete flipping of the Bloch vector from $-w$ to w.

This resonant case also leads to a simple solution of the Bloch equations. With arbitrary initial coordinates for the Bloch vector $\mathbf{u}_0 = (u_0, v_0, w_0)$ equation (3.23), can be written as

$$\mathbf{u}(t) = \mathbf{\Theta}(t) \cdot \mathbf{u}_0. \tag{3.30}$$

The matrix

$$\mathbf{\Theta}(t) = \begin{pmatrix} 1 & 0 & 0 \\ 0 & \cos\theta(t) & \sin\theta(t) \\ 0 & -\sin\theta(t) & \cos\theta(t) \end{pmatrix} \tag{3.31}$$

describes a rotation of an angle $\theta(t)$ around the u-axis. This angle is the rotation angle of the Bloch vector and is defined by the time integral of the Rabi frequency

$$\theta(t) = \int_0^t \Omega_R(t')dt'. \tag{3.32}$$

Three important cases exist:

$\pi/2$ **Pulse**
: Here the rotation angle $\theta(t)$ covers an area of $\pi/2$ and the rotation matrix reduces to

$$\mathbf{\Theta} = \begin{pmatrix} 1 & 0 & 0 \\ 0 & 0 & 1 \\ 0 & -1 & 0 \end{pmatrix}. \tag{3.33}$$

It is easy to see that this rotation flips the v and w component of the Bloch vector. Hence a superposition of both states is achieved, if the atom was initially prepared in either state $|e\rangle$ or $|g\rangle$. The Bloch vector resides in the uv-plane of the so called Bloch sphere.

π Pulse

In case of $\theta = \pi$ the rotation matrix reduces to

$$\mathbf{\Theta} = \begin{pmatrix} 1 & 0 & 0 \\ 0 & -1 & 0 \\ 0 & 0 & -1 \end{pmatrix}. \tag{3.34}$$

This infers that v_0 is transferred into $-v_0$ and w_0 into $-w_0$, which means that a population transfer takes place. If the system was initially in state $|g\rangle$ a population transfer occurs into state $|e\rangle$. It should be noted again that a complete transfer is only possible in the resonant case.

Free precession

In absence of a driving field ($\Omega_R = 0$) the Bloch vector rotates with frequency δ around the w axis of the Bloch sphere. Its evolution in time t is described by the rotation matrix $\mathbf{\Phi}_{free}$

$$\mathbf{u} = \mathbf{\Phi}_{free}(t)\mathbf{u}_0 \tag{3.35}$$

with

$$\Phi_{free}(t) = \begin{pmatrix} \cos\phi(t) & \sin\phi(t) & 0 \\ -\sin\phi(t) & \cos\phi(t) & 0 \\ 0 & 0 & 1 \end{pmatrix}. \tag{3.36}$$

During the free evolution of the Bloch vector it accumulates a phase $\phi(t)$, which is represented by the total precession angle $\phi(\delta, t)$:

$$\phi(t) = \int_0^t \delta(t')dt' \tag{3.37}$$

In the next section these special cases are used to describe the experimental methods.

3.2 Experimental methods

3.2.1 Laser and microwave setup

The setup for the experiments remains mainly the same as in the other parts of the thesis. Only few modifications are done such as the implementation of a few new laser beams to optically pump the Cs atoms in the $|3, 3\rangle$ state. The guiding magnetic field needed for optical pumping is provided by the so called optical pumping coils from the Rb setup (see [26]), which also provide the quantisation axis. A microwave antenna is placed near the glass cell to perform the microwave measurements.

Laser system

In addition to the MOT beams, the lattice and the running wave trap, optical pumping beams and a so called push out beam are implemented in the main setup.

MOT laser As in the previous chapters, the closed transition of $F = 4$ to $F' = 5$ is used as the cooling transition. The laser power is provided by a Tapered Amplifier system (Sacher Lasersystems), which is locked onto the $F = 4$ to $F' = 3$ transition by polarisation spectroscopy. In order to obtain the desired transition the laser frequency is shifted by an AOM, which is also used to control the atom number and the fluorescence per atom during the experimental cycle. The repumping laser runs on the $F = 3$ to $F' = 4$ transition and pumps the lost atoms in $F = 3$ back into the cooling cycle. It is overlapped with the cooling laser beam via a PBS and transmitted to the experiment by the same fibre.

Optical pumping beam The optical pumping of Cs is performed with two different beams. For the first beam a diode laser, which is locked onto the $F = 4$ to crossover $F' = 4/5$ transition, is used. With an AOM the frequency is shifted by 125.5 MHz to the frequency of the $F = 4$ to $F' = 4$ transition. The beam is shined in on the lattice axis using π-polarised light.
The second beam is realised in diverting part of the light of the repumping laser, which is then frequency shifted to the $F = 3$ to $F' = 3$ transition. This laser is shined in along the axis of the radial dipole trap beam and consists of σ^+-polarised light.

Push out beam For state selective detection it is important to remove the atoms which are not in the state of interest. Therefore the so called push out laser which runs on the $F = 4$ to $F' = 5$ transition is used. It removes all atoms in the $F = 4$ state but leaves the atoms in $F = 3$ unaffected. The beam is provided by the same laser which is used for the first optical pumping beam. In this case the frequency is shifted with a double pass setup of the AOM. This beam is overlapped with the second beam of the optical pumping and is therefore shined in on the radial axis of the dipole trap.

Microwave setup

The ground state hyperfine splitting between $F = 3$ and $F = 4$ of Cs is nearly 9.2 GHz [31]. In order to generate the microwave pulses a synthesiser (Agilent 83751A, 0.01-20 GHz, from now on referred to as synthesiser) is used, which is connected to the LO-Input of the mixer (Mixer model: Mini Circuits ZMX-10G+, 3700-10000 MHz) and the signal is then mixed with 50 MHz (IF-Input of the Mixer) from a Rhode and Schwarz signal generator (from now on referred to as signal generator). Both, the signal generator and the synthesiser are locked onto the 10 MHz Rubidium frequency standard. For Ramsey

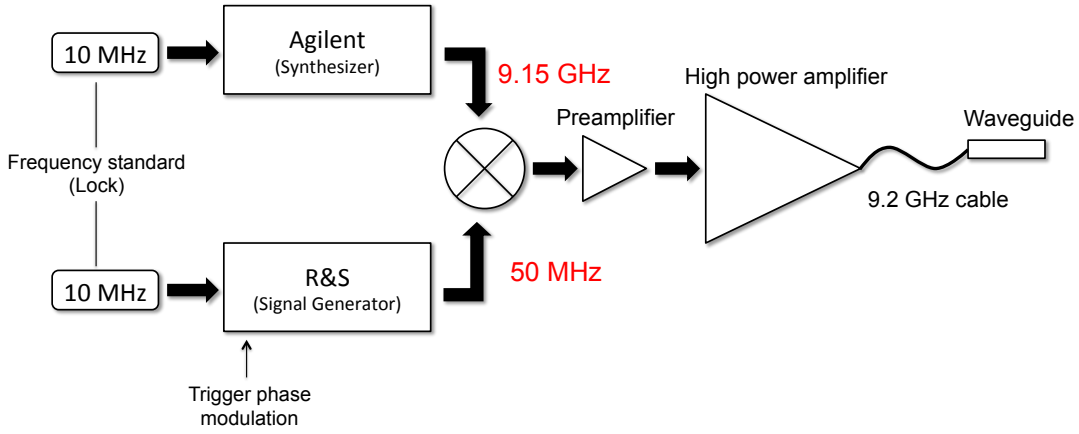

Figure 3.2: The setup used to generate the microwave signals. The signals from the Rhode and Schwarz signal generator and the Agilent synthesiser are mixed and then amplified. A low loss cable and a waveguide transmit the signal to the atoms.

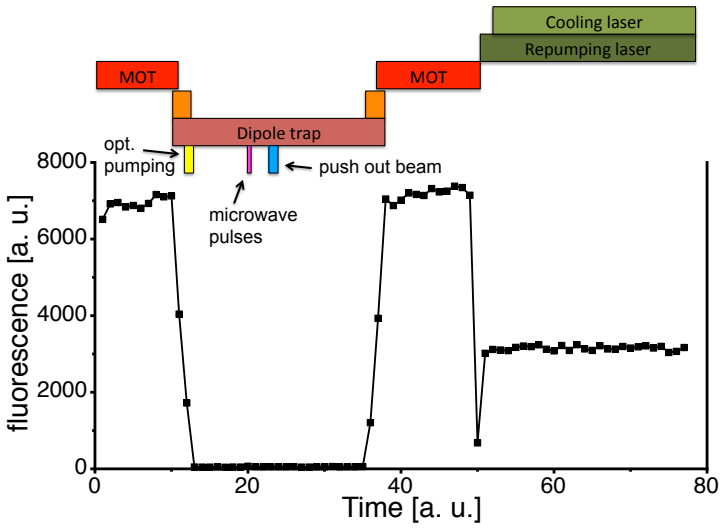

Figure 3.3: Sequence used for the different measurements involving microwave pulses. The beginning of the sequence remains the same as in the last chapters. The atoms are stored in the running wave trap or the lattice depending on the particular measurement. First the atoms are optically pumped into the desired $|3, 3\rangle$ state and then the microwave pulse is applied. After a short storage time, the push out beam removes the atoms in state $F = 4$ from the trap. The rest of the sequence remains the same as in the last chapters.

spectroscopy it is in this case necessary to have access to phase modulation (see chapter 4.3). It is decided to use mixing of the signals as this is the simplest way to obtain phase modulation, which can only be provided by the signal generator.

Both devices are operated in the cw mode, but while the signal generator delivers a continuous signal, the synthesiser resides in the trigger mode. It is remote-controlled by a computer and a signal is only generated if the synthesiser receives a trigger signal. The generated signal is then pre-amplified (Amplifier model: Kuhne Electronics, KU LNA 922 A HEMT-220) and finally sent to a power amplifier (Industrial Electronics, AM53-9-9.4-33-35), which is connected to a waveguide (see figure 3.2). In the end a power of 4 W is achieved for the microwave pulse. To avoid high losses, short cables, which are specified for microwave frequencies (Coax Multiflex 141, attenuation at 9.9 GHz: 1.45 dB/m), are used. The high power amplifier is connected to the wave guide via a -3.5 dB cable with a length of 0.5 m.

3.2.2 Experimental sequence

Again the previously introduced experimental cycle with the transfer processes into the lattice and the running wave trap is applied. It is however extended by the use of optical pumping of the Cs atoms, application of microwave pulses and the push out beam. The measurements are performed in both traps, in the lowered lattice and in the running wave trap, respectively. However, the experimental cycle in figure 3.3 is only shown for the running wave but remains the same in the lattice (except of the transfer in the running wave trap). Off-resonant Raman scattering destroys the Zeeman state preparation, hence optical pumping into the $|3,3\rangle$ state of Cs takes place directly after lowering the lattice potential resulting in a lower photon scattering rate. Details about the Raman scattering are given in section 4.2.

After optical pumping the atoms are stored in the lattice or the running wave trap, respectively. During the storage an external magnetic field is applied and microwave pulses are used to manipulate the atoms. The number of pulses as well as the duration of the pulses depend on the particular experiment. In order to know the exact hyperfine state in which the atom resides, the push out beam is used as a means of state selective detection, leading to the removal of atoms in the $F = 4$ state. Note that the push out beam only acts on the hyperfine state F and not to the particular Zeeman state m_f, which is only resolvable with microwave spectroscopy for single atoms.

3.3 Microwave spectroscopy

An essential point is to understand the influence of an external magnetic field on the level structure of an atom. In absence of an external magnetic field the hyperfine states

are degenerated. If an external magnetic field is present, the degeneracy is removed and the hyperfine states F split into $2F + 1$ sub levels. In this case the interesting states are the $F = 3$ and $F = 4$ states, which split into 7 and 9 sublevels respectively. The splitting depends directly on the strength of the applied external field. Only for small magnetic fields B < 20 G, where the energy shift is small compared to the hyperfine splitting, F is still a good quantum number. The energy shift is given by the analytic Breit-Rabi formula [43]

$$\Delta E_{F,m_F} = -\frac{\Delta E_{\text{hfs}}}{2(2I+2)} - g_I \mu_B m_F B \pm \frac{\Delta E_{\text{hfs}}}{2}\sqrt{1 + \frac{4m_F}{2I+1}x + x^2} \tag{3.38}$$

with the hyperfine splitting ΔE_{hfs}, $m = m_i \pm m_j$ and x given by

$$x = \frac{(g_I - g_J)\mu_B B}{\Delta E_{\text{hfs}}}, \tag{3.39}$$

where g_J and g_I denote the Landé factors. Cs atoms have a nuclear spin of $I = 7/2$, the hyperfine splitting is $\Delta E_{\text{hfs}} = 9.2$ GHz and the Lande factors are $g_J = 2.0$ and $g_I = -0.4 \times 10^{-3}$, respectively [31].

The shift of the transition from m_3 to m_4 due to the linear Zeeman effect is given by [31]

$$\Delta\omega_{m_3 \to m_4} = 2\pi \times 3.51 \ \frac{\text{kHz}}{\mu\text{T}} \ (m_3 + m_4) \tag{3.40}$$

and corresponds to a shift of $2\pi \times 17.55 \ \frac{\text{kHz}}{\mu\text{T}}$ for the $|3,3\rangle$ to $|4,2\rangle$ transition.

Measuring the microwave spectrum of the $|3,3\rangle \to |4,2\rangle$ transition

The atoms are prepared in the absolute ground state, i.e. $|3,3\rangle$ and the measurements are performed in the lattice as well as in the running wave trap, as explained in the previous parts of this chapter. In the running wave trap the measurements are performed with a power of $P_{\text{axial}} = 2.0$ W in axial direction and $P_{\text{radial}} = 1.5$ W in radial direction. In the lattice each beam has a power of $P_{\text{lattice}} = 100$ mW.

In order to perform microwave spectroscopy the microwave frequency of the applied pulse is stepwise scanned. The total span of the frequency is 90 kHz with a step size of 3 kHz in the running wave and 1 kHz in the lattice. For the measurements in the lattice a more simple microwave setup was used, consisting only of the Agilent synthesiser without mixing of the 50 MHz signal. In the running wave trap, the previously explained setup (sec 3.2.1) was used and the frequency of the signal from the signal generator was held stable at 50 MHz whereas the frequency of the synthesiser was varied.

Depending on the microwave frequency the pulse transfers the atoms into the $|4,2\rangle$ state,

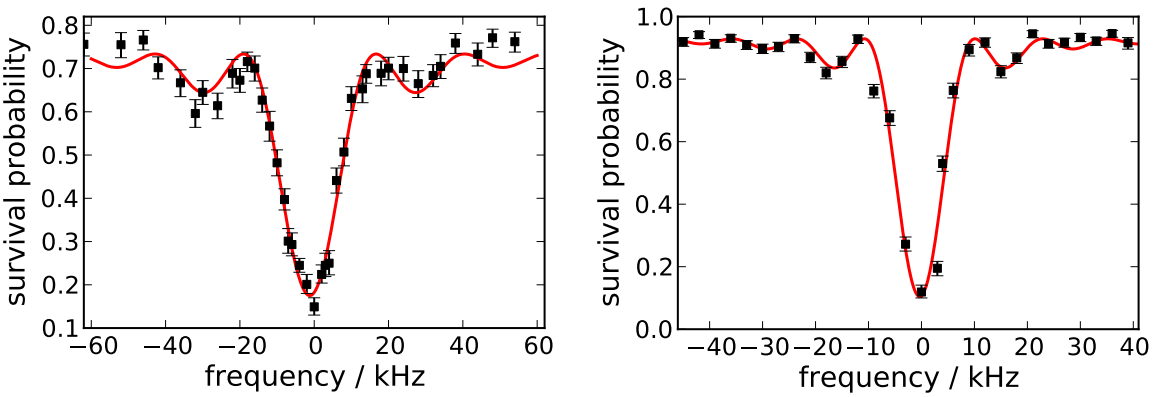

Figure 3.4: The graphs show the survival probability for atoms in the $|3,3\rangle$ state versus the microwave frequency relative to the resonance frequency. The left measurement belongs to atoms in the lattice, whereas the right one is a measurement of the microwave spectrum in the running wave. Crossing the resonance frequency leads to the dip, because all atoms are transferred in the $|4,2\rangle$ state and therefore removed from the trap by the state selective detection. A sine squared curve is fitted to the data and is shown here as the red line (see text).

Parameter	Notation	Lattice	Dipole Trap
total population transfer	A	0.59 ± 0.04	0.83 ± 0.03
Rabi frequency	$\Omega_R/2\pi$	(4947 ± 449) Hz	(2359 ± 416) Hz
pulse duration	$t/2$	(58 ± 2) µs	(100 ± 5) µs
offset	B	-0.26 ± 0.01	-0.07 ± 0.01

Table 3.1: Fit parameter for the microwave spectra of the lattice and the running wave, respectively.

leading to the spectra shown in figure 3.4. By fitting the following function resulting from the Rabi formula (eq.3.27) to the data points [42]

$$P_3(\omega) = 1 - (A \cdot \frac{\Omega_R^2}{\Omega^2} \sin^2(\frac{\Omega^2 t}{2})) + B \quad \text{with} \quad \Omega^2 = \Omega_R^2 + (2\pi(\delta - \delta_s))^2 \tag{3.41}$$

one obtains the parameters summarised in table 3.1. The large offset in the lattice arises due to imperfections of the optical pumping process resulting in the fact that a few atoms are lost and one therefore only reaches about 80% survival probability in the lattice. Optimisation of the process leads to the small offset in the running wave trap. Due to the slightly different microwave setups, a smaller coupling strength is achieved in the running wave trap. Thus the Rabi oscillations are slower and the π-pulse duration is a bit longer compared to the values for the lattice. A pulse duration of 58 µs in the lattice and 100 µs in the dipole trap, respectively, leads to a Fourier limited spectrum in

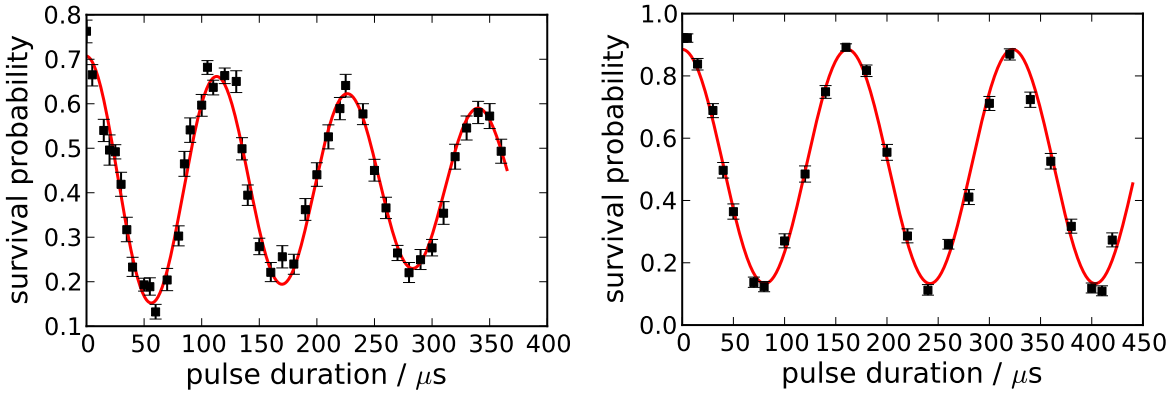

Figure 3.5: (Left) Rabi oscillations in the lattice. **(Right)** Rabi oscillations in the running wave trap. Survival probability for atoms in the $|3,3\rangle$ state versus the pulse duration of the microwave pulse. A fit of a cosine, indicated by the red line, to the data yields a Rabi frequency of $2\pi \times (8.8 \pm 0.03)$ kHz for atoms stored in the lattice and a frequency of $2\pi \times (6.2 \pm 0.02)$ kHz for atoms stored in the running wave trap. This leads to π pulse durations of approximately 56 µs and 80 µs, respectvely.

both traps.

With knowledge of the width of the Fourier limited spectrum, one can obtain a lower bound for the resolution of the applied magnetic field. In the running wave trap, a pulse with a duration of 100 µs was applied and hence a width of 10 kHz was measured. By use of the theoretical value of equation (3.40) and the width $\Delta\omega_{\mathrm{rs}}$ of the measured spectra, the minimum resolution is inferred:

$$\Delta B_{\mathrm{res}} = \frac{\Delta\omega_{\mathrm{rs}}}{2\pi \times \Delta\omega_{\mathrm{m_3 \to m_4}}} = \frac{2\pi \times 10\,\mathrm{kHz}}{2\pi \times 17.55\,\frac{\mathrm{kHz}}{\mu\mathrm{T}}} = 0.57\,\mu\mathrm{T}\,. \tag{3.42}$$

3.4 Rabi oscillations

Since the exact resonance frequency of the transition is known, one can measure the Rabi frequency in both traps. The trap parameters stay the same as in the last section. Again the transition $|3,3\rangle \to |4,2\rangle$ is driven by the microwave pulse, with the full power of 4 W and the frequency of the signal is set to the measured resonance frequency. The pulse duration is varied from 0 to 425 µs in steps of 25 µs. As in this case the resonance frequency is used, the time evolution follows from equation (3.29), which is a solution of the Bloch equations. Hence, the population in $F = 3$ can be calculated with [42]

$$P_3(t) = \frac{C}{2}\cos(\Omega_R t)\exp(-t) + B. \tag{3.43}$$

Parameter	Notation	Lattice	Dipole Trap
total population transfer	C	0.58 ± 0.03	0.82 ± 0.03
π pulse duration	$t/2$	(56.5 ± 0.2) µs	(80.5 ± 0.3) µs
Rabi oscillation	$\Omega_R/2\pi$	(8.8 ± 0.03) kHz	(6.2 ± 0.02) kHz
offset	B	0.4 ± 0.01	0.5 ± 0.01

Table 3.2: Fit parameter for the Rabi oscillations of the lattice and the running wave trap, respectively.

The measured oscillations are shown in figure 3.5 and the obtained fit parameters are summarised in table 3.2. Due to imperfections in the optical pumping process and the state selective detection, respectively, a reduced contrast results. The damping of the Rabi oscillations in the lattice arises due to an inhomogeneous decay time in the order of a π-pulse duration and is discussed in the next chapter.

3.5 Conclusion

In this chapter, the experimental details to control the internal degree of freedom have been demonstrated. The Bloch vector model was introduced and served as a theoretical model to describe the experimental techniques. By use of microwave radiation of approximately 9.2 GHz the transition of $|3,3\rangle \rightarrow |4,2\rangle$ was driven and probed by means of microwave spectroscopy. On this transition also Rabi oscillations were observed, which allow to infer the duration of a π- and $\pi/2$- pulse. These are important prerequisites in order to perform Ramsey spectroscopy and spin echo, as explained in the next chapter.

4 Measuring the coherence time of a single Cs atom

A closed quantum system without any interaction has a coherence time of infinity. However, real quantum systems always couple to their environment and therefore the coherence decays. The different decay constants, which are discussed in this chapter, are implemented in the optical Bloch equations as damping terms. This decay constants, directly corresponding to the so called coherence times, are investigated by use of Ramsey spectroscopy and spin echo techniques as described in this chapter.

With the knowledge of the π-pulse duration and the transition frequency of the states $|3,3\rangle \rightarrow |4,2\rangle$ obtained in the last chapter, it is possible to control the internal degree of freedom of the single atom. The microwave setup is now used to create a superposition between both states representing a quantum system.

4.1 Classification of decoherence effects

Data acquisition and analysis relies on the observation of an ensemble average of quantum states. In such systems decoherence manifests itself in the decay of the measured macroscopic polarisation or the dephasing of the relative phase. This is caused by various effects, but it is however reasonable to classify these as either *homogeneous* or *inhomogeneous* dephasing. Homogeneous dephasing mechanisms affect each atom of the ensemble in the same way. In contrast inhomogeneous dephasing only appears if every atom in the ensemble possesses a slightly different resonance frequency. Practically the most important difference between both effects lies in the reversibility. While inhomogeneous dephasing can be reversed using a spin echo technique, homogeneous dephasing is irreversible and also inevitable. This means that homogeneous dephasing is the limiting factor for long coherence times.

Optical Bloch equations with damping

Because real quantum systems always couple to the environment, the initial state decays with time. Hence the Bloch equations introduced in chapter 3.1 need to be extended to describe a real quantum system. The decay rates are included as damping terms into

Name	Symbol	Dominant effects
population decay time (= longitudinal decay time), irreversible	T_1	Mixing of hyperfine and Zeeman states due to off resonant Raman scattering
homogeneous dephasing time (=transverse decay time), irreversible	T_2'	variations of differential light shift (caused by pointing instability of the trap laser or magnetic field fluctuations)
inhomogeneous dephasing time, reversible	T_2^*	distribution of differential light shift
total transverse decay time	T_2	$1/T_2 = 1/T_2^* + 1/T_2'$

Table 4.1: Summary of the different decay constants and their main sources.

the Bloch equations for an atom ensemble average

$$\langle \dot{u} \rangle = \delta \langle v \rangle - \frac{\langle u \rangle}{T_2} \tag{4.1}$$

$$\langle \dot{v} \rangle = -\delta \langle u \rangle + \Omega_R \langle w \rangle - \frac{\langle v \rangle}{T_2} \tag{4.2}$$

$$\langle \dot{w} \rangle = -\Omega_R \langle v \rangle - \frac{\langle w \rangle - w_{\mathrm{eq}}}{T_1} \,. \tag{4.3}$$

Here $\langle ... \rangle$ denotes the ensemble average. The homogenous longitudinal relaxation time T_1 and transversal decay time T_2 have been introduced. T_1 corresponds to the population decay to a stationary value w_{eq} and hence to a loss of "polarisation". In contrast T_2 only affects the relative phase and preserves the population. T_2 is made up of two different components, the inhomogeneous dephasing time T_2^* and the homogenous dephasing time T_2'. They are connected via the following relation

$$\frac{1}{T_2} = \frac{1}{T_2^*} + \frac{1}{T_2'}. \tag{4.4}$$

With knowledge about all three relaxation times, summarised in table 4.1, it is possible to predict the whole evolution of an initially pure quantum system into a mixed state.

The dominant effect causing the longitudinal relaxation time T_1 is in this case spontaneous photon scattering from the light field of the lattice and the dipole trap laser. Due to Raman scattering the hyperfine and Zeeman states become distributed over all possible states of an atom ensemble and the initially prepared polarised state is destroyed. The effect is indeed observable for experiments performed in the rather near

resonant lattice potential and was measured for different trap depths (see section 4.2), such that the T_1 time can be estimated.

T_2^* is the inhomogeneous and therefore reversible dephasing time. It is dominated by the initial energy distribution of the atoms and results in a distribution of the light shifts with respect to the initial temperature of the atom. This leads to slightly different resonance frequencies for each atom and causes a phase decay.

The polarisation decay time, denoted by T_2', is mostly affected by fluctuations of experimental parameters during the experimental cycle. Such parameters are the laser intensity or the differential light shift, which are varying because of technical imperfections like the pointing instability of the lattice and the running wave trap laser. Another point is the influence of fluctuating magnetic fields. Variations may arise from current fluctuations in the coils, which create the magnetic traps or from magnetic stray fields produced by electrical devices in the lab.
A common way to measure the components of the T_2 time is Ramsey spectroscopy and variations of this method.

4.2 Measuring the population decay time

Scattering of photons from the trap laser results in population relaxation of the two ground states and is characterised by the decay time T_1.
In an optical dipole trap, such as the lattice or the running wave trap, photon scattering is inevitable [42, 44, 45]. Whereas in most cases the photons are elastically scattered (namely Rayleigh scattering), which preserves the hyperfine state, a small fraction of photons are scattered inelastically. This process, so called off-resonant Raman scattering, can result in a change of hyperfine or Zeeman level. In the present case the initial state is the $|3,3\rangle$ state and the possible final states are all Zeeman sublevels of the F = 3 and F = 4 states.
The photon scattering rate is anti-proportional to the detuning of the dipole laser with respect to the D-lines of the Cs atom, which means that for small detunings a high scattering rate is obtained. Due to the detuning of only 5 nm of the lattice laser from the Cs D1-line [31], one expects a high scattering rate of a few 100 kHz and hence a short T_1 time.

To measure the population relaxation, atoms are either prepared in the $F = 3$ or in the $F = 4$ state. The atoms are then stored in the trap for a certain time, before the state selective detection reveals the number of remaining atoms in state $F = 3$. In the lattice one observes an exponential decay of the survival probability for atoms initially prepared in $F = 3$ and an exponential increase of the survival probability for atoms initially prepared in $F = 4$. Figure 4.1 shows the measured survival probability for atoms

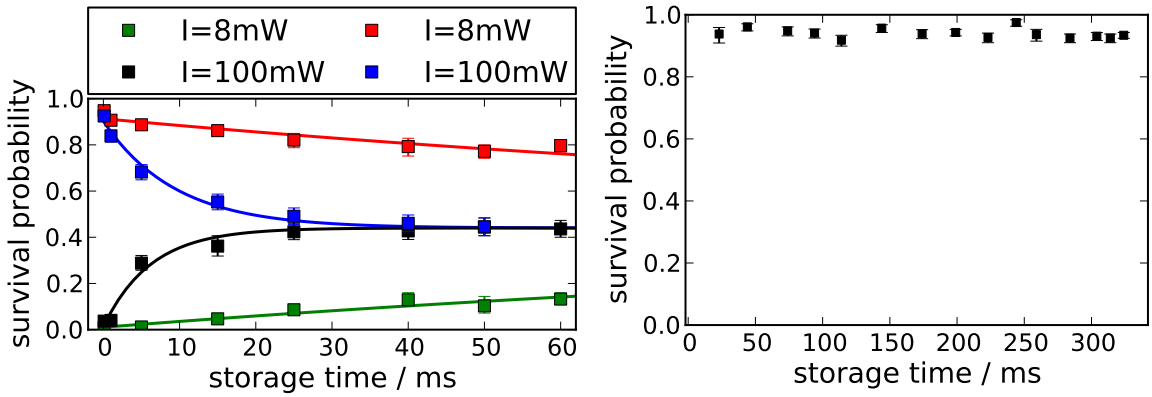

Figure 4.1: The **left** picture shows the survival probability for the atoms prepared in different hyperfine sates versus the storage time in the lattice ($\lambda = 899.9\,\mathrm{nm}$). The red and the blue line indicate atoms prepared in $F = 3$ and the black as well as green indicate atoms prepared in $F = 4$, respectively. On the **right** site the same measurement for atoms prepared in $F = 3$, which are stored in the running wave ($\lambda = 1064\,\mathrm{nm}$), is depicted.

in the lattice and the running wave. Two measurements were performed in the lattice, one with 100 mW power in each beam and another with a lowered trap using 8 mW per beam. A fit of

$$p(t) = a + p_0 \exp(-t/T_1) \tag{4.5}$$

to the data points measured in the lattice reveals a T_1 time of approximately $T_1(100\,\mathrm{mW}) = 10\,\mathrm{ms}$ for the deep lattice and approximately $T_1(8\mathrm{mW}) = 155\,\mathrm{ms}$ in the lowered lattice. For p_0 denoting the limit one obtains for atoms initially prepared in $F = 3$ a value of $p_0 = 0.47$ and for atoms prepared in F=4 a value of $p_0 = 0.43$, yielding an equal mixture of both hyperfine states.

In the running wave trap no decay on relevant time scales for atoms prepared in state $F = 3$ is observed. Hence the T_1 time is not the limiting factor for the coherence time measured in the running wave trap. The following measurements are carried out in the lowered lattice, where the T_1 time is in the order of 150 ms. As will be demonstrated in the next sections, the T_1 time is not the limiting coherence time.

4.3 Ramsey spectroscopy

Ramsey spectroscopy is an ideal and well known technique to investigate the coherence properties of a quantum system. It was first performed in the 1980s on molecular and atomic beams [46, 47]. The principle is to apply two $\pi/2$ pulses (realised here with the microwave setup) separated by a waiting time and then detect the atoms in a particular

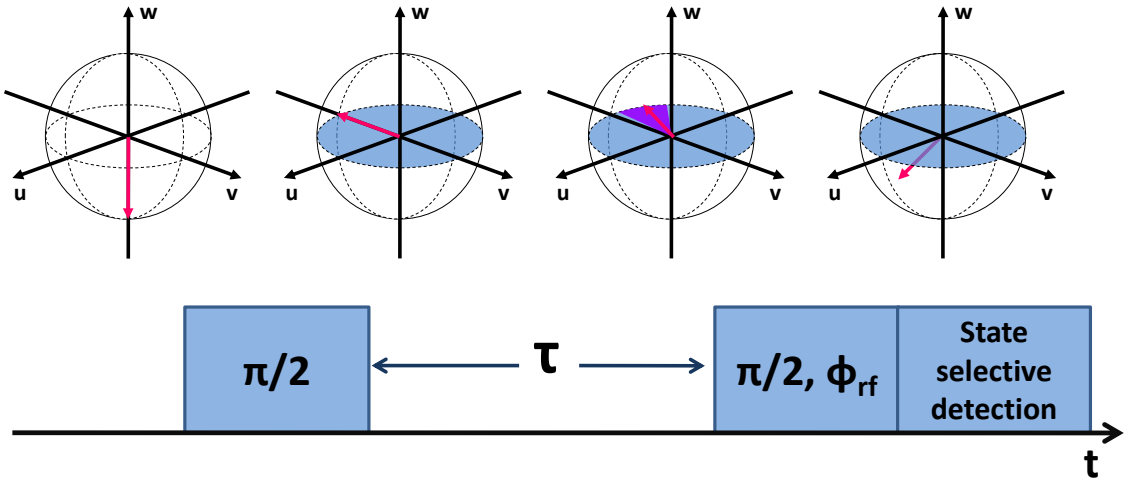

Figure 4.2: Ramsey spectroscopy illustrated for one atom of the ensemble. Initially the Bloch vectors point downwards, corresponding to atoms prepared in state $|3,3\rangle$. A $\pi/2$ pulse flips the Bloch vector into the uv-plane and a superposition between states $|3,3\rangle$ and $|4,2\rangle$ is generated. During the waiting time τ each Bloch vector of the ensemble precesses freely. The dephasing is indicated by the purple area. With a second $\pi/2$ pulse possessing a preset phase with respect to the first one, the accumulated phase is mapped on the w-axis and probed by state selective detection.

state. Today it is the key technique for atomic clocks [48], because of the sensitivity to phase shifts between the atomic resonance frequency and the driving field. The beat signal between the driving field and the atomic resonance frequency, which is the commonly detected signal, is also known as Ramsey fringe.
For the experiments the so called Ramsey phase spectroscopy method was employed. An experimental advantage of this method is that it also works with low Rabi frequencies due to the on resonance driving of the Bloch vector.

4.3.1 Experiment

Picture in the Bloch vector model

Ramsey spectroscopy uses two resonant $\pi/2$-pulses separated by a time interval τ, the so called Ramsey time. The second pulse has a phase ϕ_{rf} with respect to the first microwave pulse, which is stepwise scanned during recording of the Ramsey fringe. From now on the case of single atoms is considered.

After preparation of the atom in the initial $|F = 3, m_f = 3\rangle$ state, corresponding to the Bloch vector $\mathbf{u}_0 = (0,0,1)$, a resonant $\pi/2$-pulse is applied, which generates a superposition of the Zeeman states $|3,3\rangle$ and $|4,2\rangle$. As illustrated in figure 4.2 the pulse

rotates the Bloch vector around the u-axis into the uv-plane of the Bloch sphere and the final Bloch vector is given by $\mathbf{u} = (0, 1, 0)$. For the time interval τ the vector freely precesses in the uv-plane and accumulates a phase $\Phi_a(\tau) = \delta \cdot \tau$, with δ the detuning between the microwave frequency and the resonance frequency of the atoms. The second $\pi/2$ pulse shifted by an initially set phase ϕ_{rf} with respect to the first pulse rotates the Bloch vector around the u-axis once again. The population in $F = 3$ is probed by state selective detection.

The matrix formalism introduced in section 3.1.1 can be used to describe the Ramsey sequence,

$$\mathbf{u}_{\mathrm{Ramsey}} = \mathbf{\Theta}_{\pi/2} \cdot \mathbf{\Phi}_{\mathrm{free}}(t) \cdot \mathbf{\Theta}_{\pi/2} \tag{4.6}$$

with $\mathbf{\Theta}_{\pi/2}$ and $\mathbf{\Phi}_{\mathrm{free}}(t)$ being known rotation matrices. The w-component depending on the accumulated phase and the Ramsey time reads

$$w_{\mathrm{Ramsey}}(\phi_{\mathrm{rf}}, \tau) = C(\tau) \cos(\phi_{\mathrm{rf}} - \Phi_a(\tau)) \tag{4.7}$$

with $C(\tau)$ the Ramsey fringe contrast. As one will see later, the last equations are used to derive the fit function for the Ramsey fringe contrast in order to obtain the inhomogeneous T_2^* time.

Experimental parameters and observations

Ramsey spectroscopy was performed in both the lattice and the running wave trap. For both measurements, already introduced techniques of state preparation and state selective detection as described previously in section 3.2.2 is used. The sequence remains the same as for microwave spectroscopy, but instead of one microwave pulse, two resonant $\pi/2$ pulses are applied. For the phase modulation of the second $\pi/2$ pulse the modulation capability of the signal generator is used. The rest of the microwave setup remains the same as in the previous chapter. From the measured Rabi oscillations a $\pi/2$ pulse duration of 30 µs in the lattice and 40 µs in the dipole trap is inferred. For the measurement in the optical lattice, the lattice depth is adiabatically lowered to 8% of its initial value to avoid a high photon scattering rate, which may cause shorter coherence times and at the same time the adiabatic lowering of the lattice potential leads to further cooling of the atoms.

To investigate the time evolution of the system and hence the T_2^* time, Ramsey fringes for varying Ramsey times are recorded. Figure 4.3 shows a sample of recorded Ramsey fringes from the lattice as well as from the dipole trap. A fit of equation (4.7) leads to the Ramsey contrast $C(\tau)$, from which the T_2^* time can be calculated.

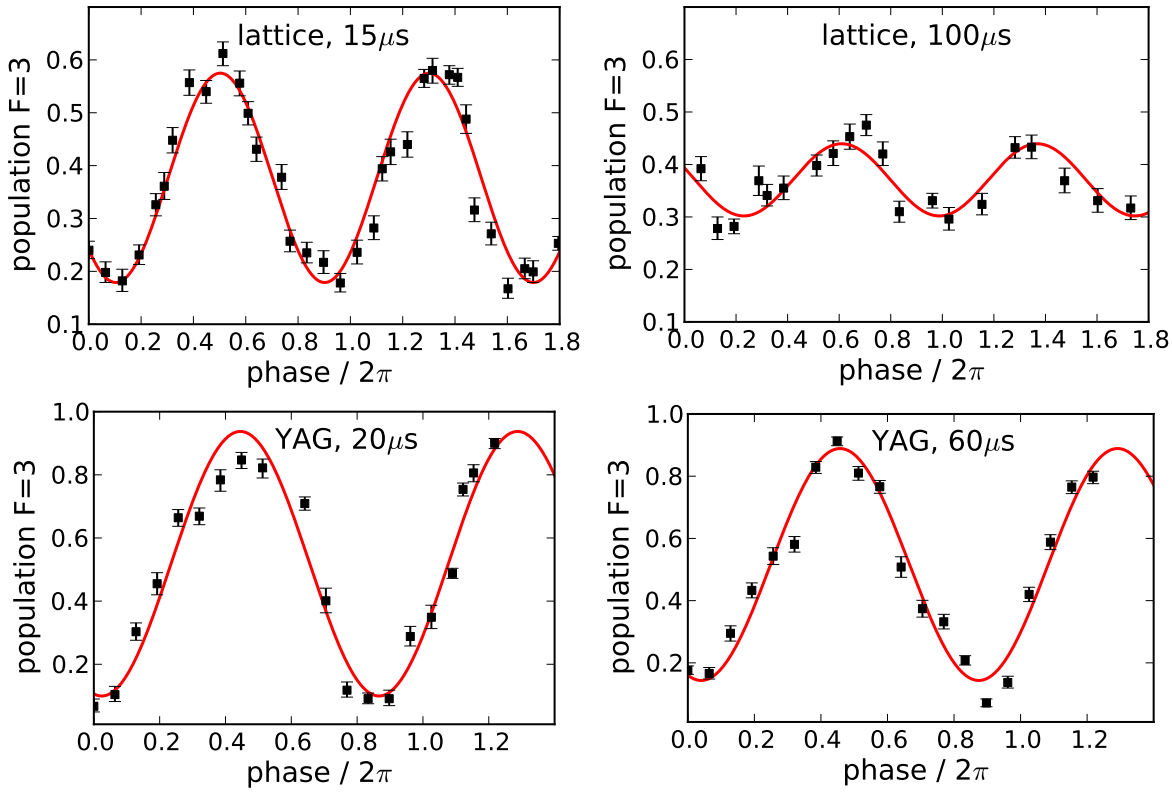

Figure 4.3: Ramsey fringes measured with different waiting times τ. A loss of contrast from $\tau = 15\,\mu s$ to $\tau = 100\,\mu s$ is clearly observable for measurements in the lattice (see upper two graphs). For measurements in the running wave trap (lower two graphs) no significant loss is observed for waiting time $\tau = 60\,\mu s$ compared to the contrast at $\tau = 20\,\mu s$.

4.3.2 Inhomogeneous dephasing

A non exponential decay is observed for the measured Ramsey contrast, which is caused by the inhomogeneous dephasing described by the characteristic decay time T_2^*. The main source for inhomogeneous dephasing is in this case the energy distribution of the trapped atoms. For different energies, the atoms experience different light shifts and hence slightly different detunings from the resonance frequency. This leads to the fact that every atom possesses a Bloch vector with a slightly different angular frequency. Because every data point of the measurement is an average over many single atom contributions, the Bloch vector dephases, which leads to a decay of the Ramsey fringe contrast for increasing waiting time τ. As will be seen in the next chapter the differential light shift is the main reason for the distributed angular frequencies.

Differential light shift

Due to the light of the laser generating the trap (the Ti:Sa or the Nd:YAG, respectively) the atoms experience a light shift, which is given via the trapping potential [29, 42]

$$U_0 = \frac{\Gamma\hbar}{8}\frac{I_{\max}}{I_0}\frac{\Gamma}{\Delta} \tag{4.8}$$

with the natural line width of the transition Γ, the detuning Δ, the saturation intensity I_0, which is $1.1\,\mathrm{mW/cm^2}$ for the Cs 6S→6P transition [31] and the maximum intensity

$$I_{\max} = \frac{4P}{\pi w_0^2} \tag{4.9}$$

with P the beam power and w_0 the beam waist. For atoms in the hyperfine state $F = 4$ the detuning from the D-line of the trap laser is 9.2 GHz less than for an atom in the state $F = 3$ leading to a slightly stronger shift for atoms in $F = 4$ and a shift of the microwave frequency of the $F = 3 \rightarrow F = 4$ transition towards smaller resonance frequencies. The difference of the light shift for atoms in different hyperfine states is called *differential light shift* and it can be calculated with

$$\hbar\delta_{\mathrm{ls}} = U_0(\Delta_{\mathrm{eff}}) - U_0(\Delta_{\mathrm{eff}} + \Delta_{\mathrm{hfs}})\,. \tag{4.10}$$

Here Δ_{eff} denotes the effective detuning of the trap laser, which is given by [42]

$$\frac{1}{\Delta_{\mathrm{eff}}} = \frac{1}{3}\left(\frac{2}{\Delta_{3/2}} + \frac{1}{\Delta_{1/2}}\right) \tag{4.11}$$

with $\Delta_J = \omega_L - \omega_J$ the detuning from the D-line transition. The hyperfine splitting is the $F = 3 \rightarrow F = 4$ transition frequency $\Delta_{\mathrm{hfs}} = 2\pi \times 9.2$ GHz $= 1.2\ \Gamma$.
For the lattice, lowered to 8% of its initial depth, with the parameters

$$\lambda = 899.9\ \mathrm{nm} \tag{4.12}$$

$$\Gamma = 2\pi \times 4.95\ \mathrm{MHz} \tag{4.13}$$

$$\Delta_{\mathrm{eff}} = 522 \times 10^3\ \Gamma \tag{4.14}$$

one obtains a maximum differential light shift of $\delta_{\mathrm{ls}} = -2\pi \times 30$ kHz. The maximum differential light shift for atoms in the running wave trap is given by $\delta_{\mathrm{ls}} = -2\pi \times 1.1$ kHz at a trap depth of $\approx 100\,\mu\mathrm{K}$ (for details see [42]). As the differential light shift is the dominant effect causing the T_2^* time, these values are used to calculate a theoretical T_2^* time, which can be compared to the measured one.

Thermal distribution and T_2^* time

Until now only atoms in the bottom of the trap with energy $E = 0$ were investigated, but one needs to take into account that the atoms have a thermal distribution. Due to

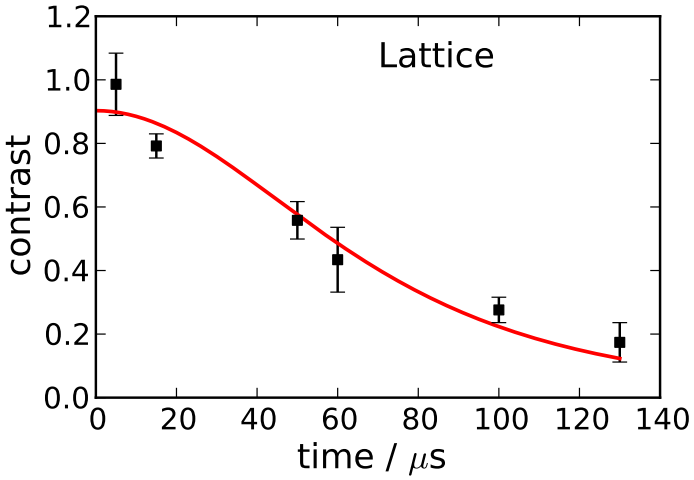

Figure 4.4: Ramsey contrast versus waiting time τ between both $\pi/2$ pulses. The red line indicates the fit of equation (4.23) to the data points. A T_2^* time of (58 ± 5) µs is obtained from the fit.

their finite temperature, every atom has a different oscillation amplitude in the trap. This leads to the fact that in general hot atoms experience a smaller light shift, because they see a lower laser intensity than cold atoms.

If an energy distribution of the trapped atoms as a three dimensional Boltzmann distribution with the probability density [28]

$$p_B(E) = \frac{E^2}{2(k_\mathrm{B}T)^3} \exp(-\frac{E}{k_\mathrm{B}T}) \tag{4.15}$$

is considered, then the distribution of differential light shifts, with an energy dependent light shift δ_ls, is given by [28]

$$p_\mathrm{ls}(\delta_\mathrm{ls}) = \frac{\beta^3}{2}(\delta_\mathrm{ls} - \delta_\mathrm{ls,0})^2 \exp[-\beta(\delta_\mathrm{ls} - \delta_\mathrm{ls,0})] \quad \text{with} \quad \beta = \frac{2U_0}{k_\mathrm{B}T\delta_\mathrm{ls,0}} \,. \tag{4.16}$$

Here T denotes the temperature of the atoms, $\delta_\mathrm{ls,0} = \delta_\mathrm{ls}(E = 0)$ is the maximum differential light shift at the bottom of the trap and U_0 is the trap depth. This equation is only valid in the regime of a harmonic approximation of the trapping potential. Equation (4.16) is in the next step used to derive an expression for the Ramsey fringe contrast in order to obtain the inhomogeneous T_2^* time.

Inferring the T_2^* time from the Ramsey contrast

The w component of Bloch vector is already known:

$$w_\mathrm{Ramsey}(\phi_\mathrm{rf}, \tau) = C(\tau)\cos(\phi_\mathrm{rf} - \Phi_a(\tau)) \,. \tag{4.17}$$

Assuming a linear evolution of the accumulated phase of each atom

$$\Phi_a(\tau) = (\delta_{\mathrm{rf}} + \delta_{\mathrm{ls}})\tau + \Phi_{\mathrm{rf},0}\,, \tag{4.18}$$

with δ_{rf} a possible frequency detuning of both $\pi/2$ pulses from the atomic transition frequency and $\Phi_{\mathrm{rf},0}$ a constant accumulated phase during the application of the pulses, one obtains an inhomogeneously broadened Ramsey signal

$$\begin{aligned} w_{\mathrm{Ramsey,inho.}}(\phi_{\mathrm{rf}}, \tau) &= \int_{\delta_{\mathrm{ls},0}}^{\infty} p_{\mathrm{ls}}(\delta'_{\mathrm{ls}}) C(\tau) \cos(\phi_{\mathrm{rf}} - (\delta_{\mathrm{rf}} + \delta'_{\mathrm{ls}})\tau - \Phi_{\mathrm{rf},0})\, d\delta'_{\mathrm{ls}} \quad (4.19) \\ &= C(\tau)\cos(\phi_{\mathrm{rf}} - \Phi(\tau))\,. \quad (4.20) \end{aligned}$$

Here $C(\tau)$ denotes the Ramsey fringe contrast and is given by

$$C(\tau) = (1 + \frac{\tau^2}{\beta^2})^{-3/2}\,. \tag{4.21}$$

Here the physically reasonable value for the upper integration limit is given by $\delta_{\mathrm{ls}}/2$, but the limit ∞ is chosen to maintain an analytical solution for the integral. Although the decay of the Ramsey fringe contrast is not exponential, the inhomogeneous dephasing time T_2^* is defined as the $1/e$ time of the Ramsey contrast

$$C(T_2^*) \equiv C(0)e^{-1} \quad \Rightarrow \quad T_2^* = \beta\sqrt{e^{2/3} - 1}. \tag{4.22}$$

By inserting equation (4.22) into equation (4.21) one obtains the fit function for the Ramsey contrast

$$C(\tau) = \left(1 + 0.948\left(\frac{\tau}{T_2^*}\right)^2\right)^{-3/2} \tag{4.23}$$

with the only fit parameter T_2^*.

The contrast inferred from Ramsey spectroscopy measurements performed in the lattice is illustrated in figure 4.4, which additionally shows the fit curve indicated by the red line. From the fit to the data points one obtains a maximum contrast of $(92 \pm 4)\%$.

The fit function yields an inhomogeneous dephasing time of

$$T_2^* = (58 \pm 5)\,\mu\mathrm{s}, \tag{4.24}$$

which is of the same order of a π-pulse time ($t = (56.5 \pm 0.5)\,\mu\mathrm{s}$) and therefore may be the dominant effect causing the observed decay of the Rabi oscillation contrast.

From the measured temperature of 30 µK in the lattice at full power the temperature

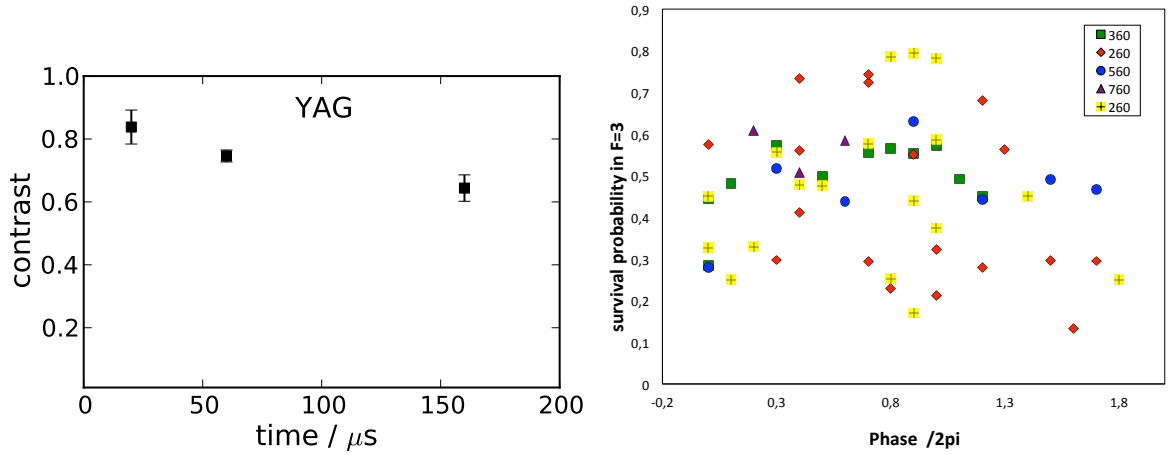

Figure 4.5: (Left) Ramsey contrast versus the waiting time τ between the two $\pi/2$ pulses. The data is obtained from measurements on atoms stored in the running wave trap. **(Right)** Ramsey fringes for different waiting times measured on atoms stored in the running wave trap. One can see that the survival probability fluctuates during the measurements. A cosine could be estimated, but it was not possible to fit any reasonable equation to the data points.

in the adiabatically lowered trap is calculated. This is possible because in a harmonic potential the fraction E/Ω, with E the sum of the potential and kinetic energy and Ω the oscillation frequency, is invariant under adiabatic changes of the trapping potential. It results in the fact that, by using the relation $\Omega \propto \sqrt{U}$, one can directly infer the temperature from the trap depth via $T(U) = T'\sqrt{U/U'}$.

With a theoretically expected value of $\delta_{\mathrm{ls}} = -2\pi \times 30$ kHz and a temperature of approximately 9 µK in the adiabatically lowered trap of trap depth $U_0 = 58$ µK an inhomogeneous dephasing time of

$$T^*_{2,\mathrm{theo}} = 66 \pm 9\ \mu\mathrm{s} \tag{4.25}$$

is calculated from equations (4.22) and (4.16). The error is calculated with propagation of uncertainty by estimating a 10% error for the temperature as well as for the trap depth. Within the error boundaries the measured value fits to the theoretically expected time. It is hence reasonable to assume that the T_2^* time in the lattice is dominated by the differential light shift.

Until now only the T_2^* time in the lattice was examined, but Ramsey spectroscopy was also performed in the running wave trap. The contrast inferred from the Ramsey fringe measured in the running wave trap, is shown in figure 4.5. Only three points are shown because for longer waiting times τ it was not possible to measure the contrast. Due to unknown effects the data points during recording of the Ramsey fringes fluctuated and

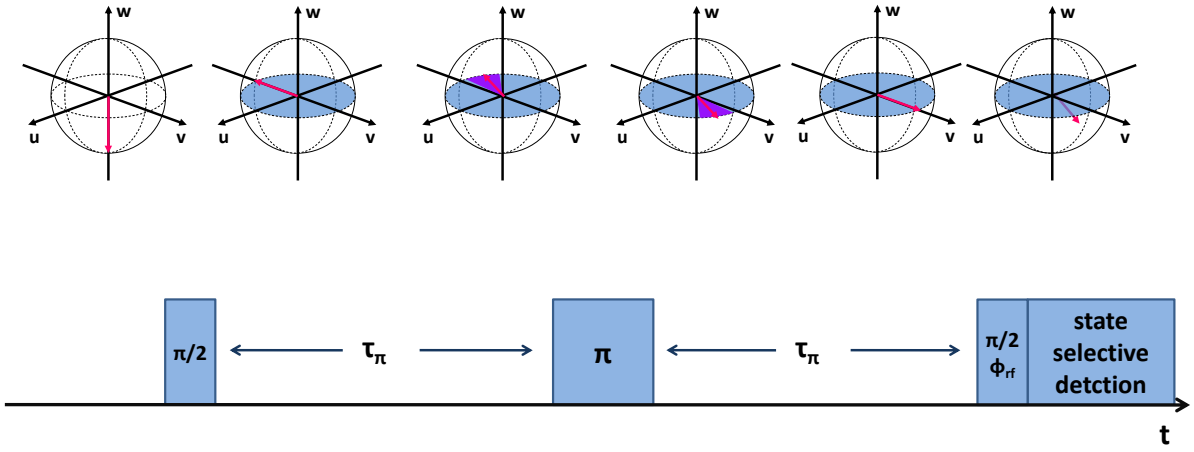

Figure 4.6: Spin echo sequence in Bloch vector model. The only difference compared to Ramsey spectroscopy is the application of an additional π pulse in the middle of the sequence, which rephases the Bloch vectors of the ensemble.

it was not possible to fit an appropriate cosine to the data points (see fig 4.5). But from the few points available one can assume a T_2^* time much longer than in the lattice. With the theoretically expected value of $2\pi \times 1.1$ kHz for the differential light shift, a measured temperature of $\approx 5\,\mu$K and a trap depth of $\approx 100\,\mu$K a theoretical value of $T^*_{2,\mathrm{theo}} = 2.8\,$ms is calculated corresponding well to the trend of the data points, but one can see that the coherence time is not limited by the T_2^* time.

4.4 Spin echo technique

Inhomogeneous dephasing can be reversed by the so called Spin-echo technique invented by E. Hahn in the 1950s originally used for nuclear magnetic resonance [49]. Since several years the method is also a standard technique for experiments with atoms in optical dipole traps [50].

For Spin-echo measurements the Ramsey spectroscopy sequence is extended by an additional π-pulse between the two $\pi/2$-pulses leading to a rephasing of the ensemble. It is used to measure the homogeneous relaxation time T_2'.

4.4.1 Experiment

Picture in the Bloch vector model

During the waiting time after the first $\pi/2$-pulse, the Bloch vectors dephase because of the reasons discussed in the previous section. The π pulse additionally applied after time τ_π rotates the Bloch vector by an angle of 180° around the u-axis of the Bloch sphere.

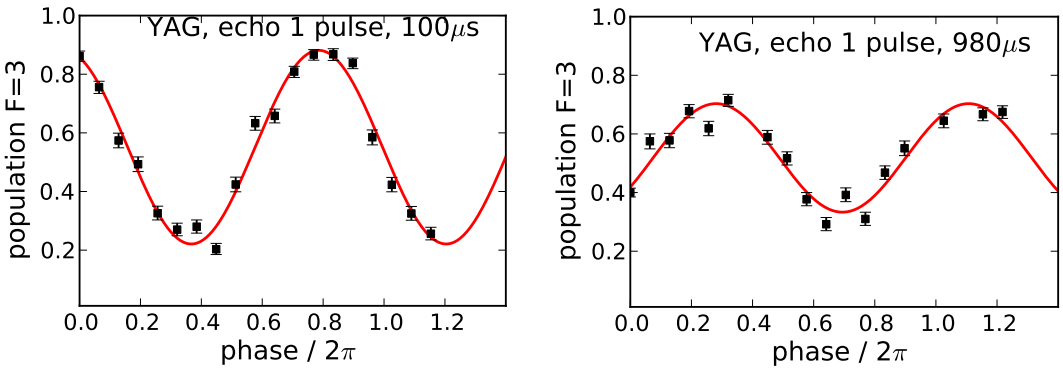

Figure 4.7: Two exemplary Ramsey fringes measured with the spin echo technique for atoms stored in the running wave trap. After a waiting time τ_π of approximately 1 ms an sufficient contrast is still observable.

This leads to a time reversal and hence the Bloch vectors are completely rephased in state $\mathbf{u} = (0, 1, 0)$ after time $2\tau_\pi$, see figure 4.6.

Because Ramsey spectroscopy and the spin echo technique are similar methods, the matrix formalism derived in section 3.1.1 is used again to describe the spin echo sequence. The evolution of the Bloch vector prepared in the initial state $\mathbf{u}_0 = (0, 0, -1)$, yields

$$\mathbf{u}_{\text{echo}}(\phi_{\text{rf}}, 2\tau_\pi) = \Theta_{\pi/2} \cdot \Phi_{\text{free},1}(\tau_\pi) \cdot \Theta_\pi \cdot \Phi_{\text{free},2}(\tau_\pi) \cdot \Theta_{\pi/2} \cdot \mathbf{u}_0 \tag{4.26}$$

with the known rotation matrices for $\Theta_{\pi/2}$, Θ_π and Φ_{free} (see section 3.1.1). For the w component we obtain from equation (4.26):

$$w_{\text{echo}} = \frac{1}{2}\left(1 + \cos[\phi_{\text{rf}} - \Delta\Phi(\tau) + \pi]\right) \tag{4.27}$$

with $\Delta\Phi = \Phi_{\text{free},1}(\tau_\pi) - \Phi_{\text{free},2}(\tau_\pi)$ the difference between the accumulated phases before and after the π pulse, respectively.

Experimental parameters and Observations

For the spin echo sequence the same experimental parameters as for Ramsey spectroscopy are employed due to similarities of the techniques. Again the transition $|3, 3\rangle \rightarrow |4, 2\rangle$ is used. The pulse length of the π-pulse is 60 µs in the lattice and 80 µs in the running wave trap, respectively. In figure 4.7 some Ramsey fringes recorded with the spin echo technique are depicted.

4.4.2 Homogeneous dephasing

In the ideal case, meaning that during the experimental cycle the individual resonance frequency of each atom stays the same, the spin echo method is able to fully reverse the

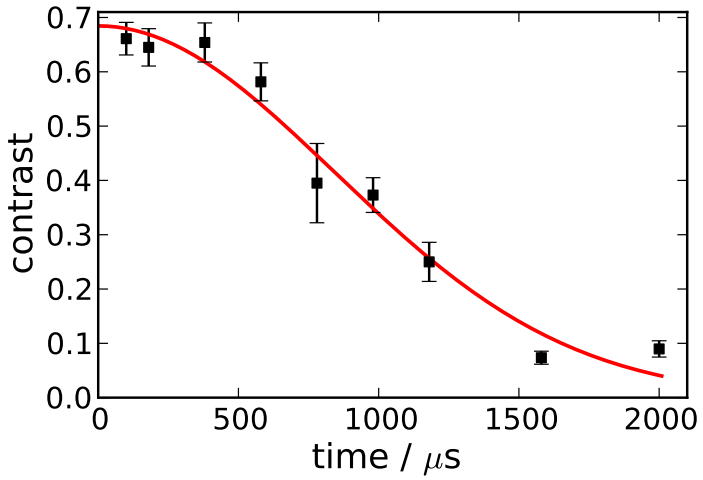

Figure 4.8: Spin echo contrast versus waiting time τ_π. The black squares indicate the data points, whereas the red solid line represents a fit of equation (4.34) to the data. A homogeneous decay time T_2' of (1.19 ± 0.06) ms is inferred from the fit.

dephasing which occurs during the time in which the Bloch vector precesses freely. The result would be a spin echo contrast of 100 %.

However, the experiments show that the spin echo contrast decays, which is due to irreversible dephasing mechanisms, denoted by the homogeneous dephasing time T_2'. Sources for such effects are fluctuations of the laser intensity or of magnetic fields during the performance of the sequence. These fluctuations lead to the fact that the accumulated phases before and after the π pulse are different. The effect is expressed by a time averaged detuning difference $\Delta\delta$ in time τ_π

$$\Delta\Phi_a(\tau_\pi) = \Delta\delta \cdot \tau_\pi. \tag{4.28}$$

A Gaussian shape for the probability distribution of the average detuning difference is assumed [28]

$$p(\Delta\delta, \tau_\pi) = \frac{1}{\sqrt{2\pi}\sigma(\tau_\pi)} \exp\left[-\frac{(\Delta\delta)^2}{2\sigma^2(\tau_\pi)}\right] \tag{4.29}$$

with mean $\overline{\Delta\delta} = 0$ and variance $\sigma^2(\tau_\pi)$. Then the homogeneously broadened spin echo signal is given by [28]

$$\begin{aligned} w_{\text{echo,homo.}}(\phi_{\text{rf}}, 2\tau_\pi) &= \int_{-\infty}^{\infty} p(\Delta\delta), \tau_\pi) C(\tau) \cos[\phi_{\text{rf}} - \Delta\delta\tau_\pi + \pi]\, d\Delta\delta & (4.30) \\ &= C(2\tau_\pi) \cos[\phi_{\text{rf}} + \pi] & (4.31) \end{aligned}$$

with the spin echo contrast

$$C(2\tau_\pi) = \exp[-\frac{1}{2}\tau_\pi^2\sigma^2(\tau_\pi)]. \tag{4.32}$$

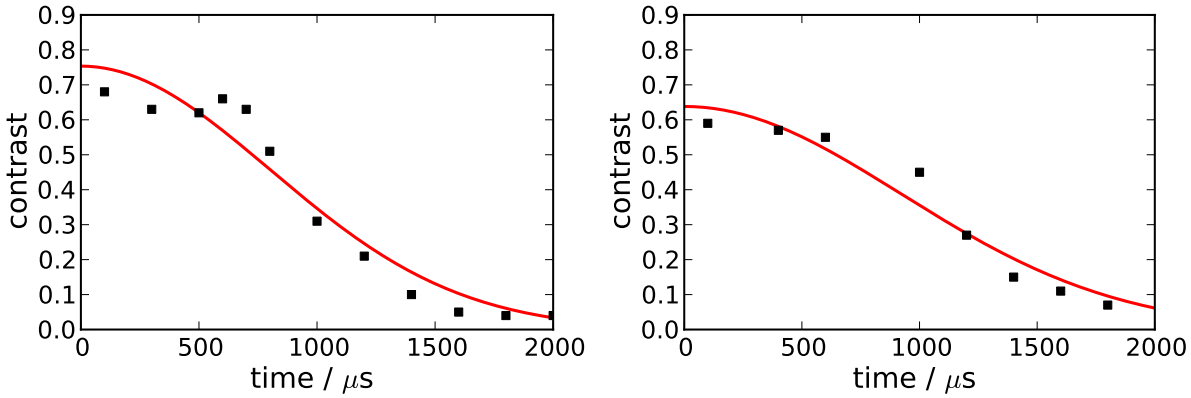

Figure 4.9: Spin echo contrast versus waiting time τ_π. The data was obtained from atoms stored in the running wave trap at a different trap depth as the first measurement. A power of $P_{\text{axial}} = 3\,\text{W}$ in axial direction and of $P_{\text{radial}} = 0.6\,\text{W}$ in radial direction was used during this measurements.

Again the T_2' time is defined as the $1/e$ time of the spin echo contrast signal

$$C(2\tau_\pi = T_2') \equiv C(0)e^{-1} \qquad \Longrightarrow \qquad T_2' = \frac{\sqrt{2}}{\sigma(\tau_\pi)}. \tag{4.33}$$

Combining the last equation with equation (4.32) and adding a fit parameter, which takes the deviation from the maximal contrast into account, leads to the used fit function of

$$C(2\tau_\pi) = C_{\max} \exp\left[-\left(\frac{\tau_\pi^2}{T_2'}\right)^2\right], \tag{4.34}$$

which directly reveals the inhomogeneous T_2' time.

The measurements were performed in the running wave trap with a power of $P_{\text{axial}} = 2\,\text{W}$ in axial direction and $P_{\text{radial}} = 1.5\,\text{W}$ in radial direction. Figure 4.8 shows the evolution of the contrast depending on the spin echo time τ_π. A dephasing time of

$$C(2\tau_\pi) = (1186 \pm 60)\,\mu\text{s} \tag{4.35}$$

is inferred from the fit resulting in a variance of

$$\sigma(\tau_\pi) = (190 \pm 10)\,\text{Hz}\,. \tag{4.36}$$

Measurements (see fig. 4.9) with a different trap depth ($P_{\text{axial}} = 3\,\text{W}$ and $P_{\text{radial}} = 0.6\,\text{W}$) yield nearly the same T_2' times, which are $T_2' = (1300 \pm 84)\,\mu\text{s}$ and $T_2' = (1129 \pm 74)\,\mu\text{s}$, respectively. Hence intensity fluctuations or pointing instability of the trap laser, causing changes of the trap depth and therefore changes of the differential light shift, are assumed not to be the limiting factors.

Analysis of dephasing mechanisms

In the next step the variances resulting from different effects are calculated and then compared to the measured one, following the methods of references [42, 28]. The deviations of the parameters are estimations in most cases.

Intensity fluctuations Fluctuations of the laser intensity of the trap laser directly affect the trap depth and hence the differential light shift. Because we need to perform the spin echo measurement about a 100 times, every atom sees a trap depth slightly different resulting in a dephasing of the Bloch vectors corresponding to each atom. Due to the fact that an electronic feed back loop is used to control the laser power in each beam independently, one is only limited by its accuracy. Therefore the fluctuations are estimated to $\epsilon = 0.5\%$ of the initial intensity.
The variance caused by the fluctuations can be calculated via

$$\frac{\sigma(\tau)}{2\pi} = \sqrt{2}\delta_{\mathrm{ls}}\epsilon \tag{4.37}$$

with ϵ the estimated variance of the parameter, rather than the Allen variance used in [42]. For a maximum light shift of $\delta_{\mathrm{ls}} = 2\pi \times 1.1$ kHz one hence obtains a variance of $\frac{\sigma(\tau)}{2\pi} = 7.8$ Hz. This is one order of magnitude too small to be the limiting effect. It corresponds well to the fact that neither the trap depth nor the differential light shift matter here.

Beam pointing instability Like intensity fluctuations the pointing instability of the laser generating the trap causes fluctuations of the trap depth and hence of the differential light shift. Here the pointing instability is estimated to be small compared to the beam waist, as one would observe a lower transfer efficiency from the lattice into the running wave otherwise. A variance of $\frac{\sigma(\tau)}{2\pi} = 31$ Hz is calculated from equation (4.37) with $\epsilon = 2\%$. This is again too small to be the limiting factor.

Magnetic field fluctuations The current through the coils generating the magnetic guiding field may be slightly unstable and hence results in fluctuations of the magnetic field. Due to the linear Zeeman shift, this is directly translated into resonance frequency shifts of the relevant transition ($|3,3\rangle \rightarrow |4,2\rangle$). The shift is in this case calculated via

$$\Delta\omega = 2B_0\Delta\omega_{\mathrm{m_3}\rightarrow\mathrm{m_4}} \tag{4.38}$$

with $B_0 = 1$ mT the applied magnetic field strength and $\Delta\omega_{\mathrm{m_3}\rightarrow\mathrm{m_4}} = 2\pi \times 3.51\frac{\mathrm{kHz}}{\mu\mathrm{T}}(m_3 + m_4) = 5 \cdot 2\pi \times 3.51\frac{\mathrm{kHz}}{\mu\mathrm{T}}$ the splitting due to the linear Zeeman shift. For the variance one obtains

$$\frac{\sigma(\tau)}{2\pi} = \sqrt{2}\Delta\omega\epsilon = 208 \text{ Hz} \tag{4.39}$$

with $\epsilon = I_{\mathrm{rms}}/I_0 = 3 \times 10^{-6}$ given by the Toellner power supply. Although the value is larger than the measured one, it is in the expected variance range and it

makes sense that the magnetic field fluctuations are the limiting factor, due to the strong dependency of the transition frequency for the outer Zeeman states on the magnetic field.

Summarising the effect limiting the inhomogeneous decay time are probably magnetic field fluctuations, because the transition frequency $|3,3\rangle \rightarrow |4,2\rangle$ strongly depends on the magnetic field. It was furthermore found the differential light shift not to be responsible for the limited coherence time in measurements for different trap depths. This statement was supported by calculations for the beam pointing instability and the laser intensity fluctuations. Note that the magnetic field fluctuations arising from electrical devices in the lab are not taken into account.

5 Conclusions and Outlook

During this thesis a species selective lattice was built and implemented in the current setup. A transfer efficiency from the single atom MOT into the lattice and back close to unity has been achieved. this is an essential prerequisite for future experiments, because all measurements rely on counting the atom number in the MOT before and after manipulation of the atom. It was verified that the measured lattice parameters agree with the theoretically predicted values. Therefore it is now used as an intermediate step for combining a single Cs atom from a dissipative trap with a many particle system of Rb atoms, which are evaporatively cooled and stored in a conservative shallow dipole trap, resulting in the demonstration of sympathetic cooling of the single atom by the Rb cloud (see [36]).

After combination of both systems it was the intention to investigate the coherence behaviour of a single superposition state during or after the interaction with the ultracold gas. The measurements being performed and introduced in this thesis are in fact the calibration of such measurements. To this end a microwave setup has been built and used to generate a superposition state of two Zeeman states in a single Cs atom.

From a Ramsey spectroscopy measurement performed in the lattice, the inhomogeneous coherence time of nearly 60 µs has been inferred and the differential light shift has been found to be the limiting factor. This time is however too small compared to the thermalisation time of 25 ms [36] to analyse a possible decay during the interaction of the single atom and the ultracold cloud. Besides the fact that the Rb cloud is stored in the dipole trap, the low differential light shift and hence a longer coherence time is another reason to use the dipole trap instead of the lattice.

Within the dipole trap we measured the homogeneous coherence time of approximately 1200 µs using different trap depths, observing that the time stays the same in each measurement. We therefore conclude that inhomogeneous effects, such as the differential light shift, are not the limiting factors. In contrast homogeneous effects limit the coherence time. The limiting processes are mainly ascribed to fluctuations of the current flowing through the coils generating the magnetic guiding field. This is reasonable because the used transition between the Zeeman states is very sensitive to magnetic fields due to the linear Zeeman effect. Although we neither use the outer most transitions we can compare our value to others measured in the group, where a time of 415 µs [28] for $|3,3\rangle \rightarrow |4,4\rangle$ transition have been observed. Referring to this measurements our coher-

ence time is much longer and is a good candidate to investigate the coherence properties of a single atom during the interaction with an ultracold gas. The thermalisation time for the Cs atom in the ultracold Rb cloud is in the order of 25 ms. Therefore on time scales of the coherence time (1 ms) it is possible to observe cooling of the superposition state. Unfortunately it was not possible to perform a combined measurement of a single Cs atom and an ultracold Rb cloud because of a major vacuum leak.

In the near future a new experimental setup will be build having an all optical BEC allowing a much faster measurement cycle (up to 6 s per BEC compared to 1 minute in the old setup). With this setup, higher Rb densities may be gained resulting in a faster thermalisation process and hence it is then possible to analyse the coherence time during combination of both systems.

Bibliography

[1] T. W. Hänsch, "Cooling of gases by laser radiation," *Optics Communications*, vol. 13, no. I, pp. 68–69, 1975.

[2] H. F. Hess, "Evaporative cooling of magnetically trapped and compressed spin-polarized hydrogen," *Phys. Rev. B*, vol. 34, pp. 3476–3479, 1986.

[3] M. H. Anderson, J. R. Ensher, M. R. Matthews, C. E. Wieman, and E. a. Cornell, "Observation of bose-einstein condensation in a dilute atomic vapor." *Science (New York, N.Y.)*, vol. 269, no. 5221, pp. 198–201, 1995.

[4] K. B. Davis, M. O. Mewes, M. R. Andrews, N. J. van Druten, D. S. Durfee, D. M. Kurn, and W. Ketterle, "Bose-einstein condensation in a gas of sodium atoms," *Phys. Rev. Lett.*, vol. 75, pp. 3969–3973, 1995.

[5] M. R. Andrews, C. G. Townsend, H.-J. Miesner, D. S. Durfee, D. M. Kurn, and W. Ketterle, "Observation of interference between two bose condensates," *Science*, vol. 275, no. 5300, pp. 637–641, 1997.

[6] I. Bloch, T. W. Hänsch, and T. Esslinger, "Atom laser with a cw output coupler," *Phys. Rev. Lett.*, vol. 82, pp. 3008–3011, 1999.

[7] K. W. Madison, F. Chevy, W. Wohlleben, and J. Dalibard, "Vortex formation in a stirred bose-einstein condensate," *Phys. Rev. Lett.*, vol. 84, pp. 806–809, 2000.

[8] S. O. Demokritov, V. E. Demidov, O. Dzyapko, G. a. Melkov, a. a. Serga, B. Hillebrands, and a. N. Slavin, "Bose-Einstein condensation of quasi-equilibrium magnons at room temperature under pumping." *Nature*, vol. 443, no. 7110, pp. 430–3, 2006.

[9] J. Klaers, J. Schmitt, F. Vewinger, and M. Weitz, "Bose-Einstein condensation of photons in an optical microcavity." *Nature*, vol. 468, no. 7323, pp. 545–8, 2010.

[10] M. Tinkham, *Introduction to Superconductivity*, 2nd ed. McGraw-Hill, 1996.

[11] R. Wynar, R. S. Freeland, D. J. Han, C. Ryu, and D. J. Heinzen, "Molecules in a bose-einstein condensate," *Science*, vol. 287, no. 5455, pp. 1016–1019, 2000.

[12] T. Kraemer, M. Mark, P. Waldburger, J. G. Danzl, C. Chin, B. Engeser, a. D. Lange, K. Pilch, a. Jaakkola, H.-C. Nägerl, and R. Grimm, "Evidence for Efimov

quantum states in an ultracold gas of caesium atoms." *Nature*, vol. 440, no. 7082, pp. 315–8, 2006.

[13] F. K. Fatemi, K. M. Jones, and P. D. Lett, "Observation of optically induced feshbach resonances in collisions of cold atoms," *Phys. Rev. Lett.*, vol. 85, pp. 4462–4465, 2000.

[14] S. Inouye, M. R. Andrews, J. Stenger, H. Miesner, and W. Ketterle, "Observation of Feshbach resonances in a Bose -Einstein condensate," *Nature*, pp. 8–11, 1998.

[15] G. Modugno, M. Modugno, F. Riboli, G. Roati, and M. Inguscio, "Two atomic species superfluid," *Phys. Rev. Lett.*, vol. 89, p. 190404, 2002.

[16] D. Schrader, S. Kuhr, W. Alt, M. Müller, V. Gomer, and D. Meschede, "An optical conveyor belt for single neutral atoms," *Applied Physics B*, vol. 73, pp. 819–824, 2001.

[17] M. Karski, L. Förster, J.-M. Choi, A. Steffen, W. Alt, D. Meschede, and A. Widera, "Quantum walk in position space with single optically trapped atoms," *Science*, vol. 325, no. 5937, pp. 174–177, 2009.

[18] A. J. Daley, P. O. Fedichev, and P. Zoller, "Single-atom cooling by superfluid immersion: A nondestructive method for qubits," *Phys. Rev. A*, vol. 69, p. 022306, 2004.

[19] A. Griessner, A. J. Daley, S. R. Clark, D. Jaksch, and P. Zoller, "Dark-state cooling of atoms by superfluid immersion," *Phys. Rev. Lett.*, vol. 97, p. 220403, 2006.

[20] J. F. Sherson, C. Weitenberg, M. Endres, M. Cheneau, I. Bloch, and S. Kuhr, "Single-atom-resolved fluorescence imaging of an atomic Mott insulator," *Nature*, vol. 467, no. 7311, pp. 68–72, 2010.

[21] T. Gericke, P. Würtz, D. Reitz, T. Langen, and H. Ott, "High-resolution scanning electron microscopy of an ultracold quantum gas," *Nature Physics*, vol. 4, no. 12, pp. 949–953, 2008.

[22] M. Bruderer and D. Jaksch, "Probing bec phase fluctuations with atomic quantum dots," *New Journal of Physics*, vol. 8, no. 6, p. 87, 2006.

[23] H. T. Ng and S. Bose, "Single-atom-aided probe of the decoherence of a bose-einstein condensate," *Phys. Rev. A*, vol. 78, p. 023610, 2008.

[24] T. Weikum, "Ein System zur Fluoreszenzdetektion einzelner Cäsiumatome in einem Rubidium Bose-Einstein-Kondensat," 2009, Diplomarbeit.

[25] C. Weber, "Controlled few-body interactions in ultracold bosonic mixtures," Ph.D. dissertation, University of Bonn, 2009.

[26] S. John, "Towards Single atom aided probing of an ultracold quantum gas," Ph.D. dissertation, University of Bonn, 2011.

[27] E. L. Raab, M. Prentiss, A. Cable, S. Chu, and D. E. Pritchard, "Trapping of neutral sodium atoms with radiation pressure," *Phys. Rev. Lett.*, vol. 59, pp. 2631–2634, 1987.

[28] M. Karski, "State-selective transport of single neutral atoms," Ph.D. dissertation, University of Bonn, 2010.

[29] R. Grimm, M. Weidemüller, and Y. B. Ovchinnikov, "Optical dipole traps for neutral atoms," in *Advances In Atomic, Molecular, and Optical Physics*, 2000, vol. 42, pp. 95 – 170.

[30] D. Meschede, *Optik, Licht und Laser*, 2nd ed. Teubner, 2005.

[31] D. A. Steck, "Cesium D Line Data," http://steck.us/alkalidata.

[32] O. Fetsch, "A species selective trap for single Cs atoms," 2010, Diplomarbeit.

[33] W. Alt, "Optical control of single neutral atoms," Ph.D. dissertation, University of Bonn, 2004.

[34] N. Spethmann, F. Kindermann, S. John, C. Weber, D. Meschede, and A. Widera, "Inserting single Cs atoms into an ultracold Rb gas," *arXiv:1109.1639v1*, 2011.

[35] M. Mudrich, S. Kraft, K. Singer, R. Grimm, A. Mosk, and M. Weidemüller, "Sympathetic cooling with two atomic species in an optical trap," *Phys. Rev. Lett.*, vol. 88, p. 253001, 2002.

[36] N. Spethmann, "Dissertation," to be published.

[37] T. Esslinger, I. Bloch, and T. W. Hänsch, "Bose-einstein condensation in a quadrupole-ioffe-configuration trap," *Phys. Rev. A*, vol. 58, pp. R2664–R2667, 1998.

[38] A. Kastler, "Optical Methods of Atomic Orientation and of Magnetic Resonance," *JOSA*, vol. 47, no. 6, pp. 460–465, 1957.

[39] T. R. Carver, "Optical Pumping." *Science (New York, N.Y.)*, vol. 141, no. 3581, pp. 599–608, 1963.

[40] F. Bloch, "Nuclear induction," *Phys. Rev.*, vol. 70, pp. 460–474, 1946.

[41] L. Allen and J. H. Eberly, *Optical Resonance and Two-Level Atoms.* Dover Publications, 1987.

[42] S. Kuhr, "A controlled quantum system of individual neutral atoms," Ph.D. dissertation, University of Bonn, 2003.

[43] G. Breit and I. I. Rabi, "Measurement of nuclear spin," *Phys. Rev.*, vol. 38, pp. 2082–2083, 1931.

[44] D. Frese, B. Ueberholz, S. Kuhr, W. Alt, D. Schrader, V. Gomer, and D. Meschede, "Single atoms in an optical dipole trap: Towards a deterministic source of cold atoms," *Physical Review Letters*, vol. 85, no. 18, pp. 3777–3780, 2000.

[45] R. a. Cline, J. D. Miller, M. R. Matthews, and D. J. Heinzen, "Spin relaxation of optically trapped atoms by light scattering." *Optics letters*, vol. 19, no. 3, p. 207, 1994.

[46] N. F. Ramsey, "A molecular beam resonance method with separated oscillating fields," *Phys. Rev.*, vol. 78, pp. 695–699, 1950.

[47] N. Ramsey, *Molecular Beams.* Oxford University Press, 1956.

[48] J. Vanier and C. Audoin, *The Quantum Physics of Atomic Frequency Standards.* Adam Hilger, 1989.

[49] E. L. Hahn, "Spin echoes," *Phys. Rev.*, vol. 80, pp. 580–594, 1950.

[50] M. F. Andersen, A. Kaplan, and N. Davidson, "Echo spectroscopy and quantum stability of trapped atoms," *Phys. Rev. Lett.*, vol. 90, p. 023001, 2003.

Danksagung

An dieser Stelle möchte ich mich bei allen bedanken, die mich während meiner Masterarbeitszeit unterstützt haben.

Zu aller erst danke ich Prof. Dr. Meschede für die Möglichkeit meine Masterarbeit an diesem spannenden Experiment anfertigen zu dürfen.

Prof. Dr. Artur Widera danke ich für die grossartige Unterstützung während meiner gesamten Masterarbeit, für die Klärung meiner physikalischer Fragen, für seine optimistische Art , für das hilfreiche Korrekturlesen meiner Arbeit und nicht zuletzt für die Übernahme des Zweitgutachtens.

Nicolas Spethmann danke ich ebenfalls für die grossartige Unterstützung während meiner gesamten Masterarbeit, für das hilfreiche Korrekturlesen dieser Arbeit, für seine geduldige Art und für das beantworten sämtlicher meiner Fragen.

Auch Claudia und Shincy, die zu Begin meiner Arbeit am Experiment mit gearbeitet haben, möchte ich ebenfalls für ihre Unterstützung danken.

Dem Rest der Arbeitsgruppe danke ich für die angenehme Atmosphäre und insbesondere Wolfgang für hilfreiche Tips während der Teepausen.

Mein ganz besonderer Dank gilt meiner Mutter und meinem Freund Philip. Beide haben mich nicht nur während meiner Masterarbeit, sondern während meiner gesamten Studienzeit und darüber hinaus ausserordentlich unterstützt. Ohne sie wäre diese Arbeit nicht möglich gewesen.

I herby certify that the work presented here was accomplished by myself and without the use of illegitimate means or support, and that no sources and tools were used other than those cited.

Bonn,